NOTICE

The quality of this microform is heavily dependent upon the quality of the original thesis submitted for microfilming. Every effort has been made to ensure the highest quality of reproduction possible.

If pages are missing, contact the university which granted the degree.

Some pages may have indistinct print especially if the original pages were typed with a poor typewriter ribbon or if the university sent us an inferior photocopy.

Reproduction in full or in part of this microform is governed by the Canadian Copyright Act, R.S.C. 1970, c. C-30, and subsequent amendments.

AVIS

La qualité de cette microforme dépend grandement de la qualité de la thèse soumise au microfilmage. Nous avons tout fait pour assurer une qualité supérieure de reproduction.

S'il manque des pages, veuillez communiquer avec l'université qui a conféré le grade.

La qualité d'impression de certaines pages peut laisser à désirer, surtout si les pages originales ont été dactylographiées à l'aide d'un ruban usé ou si l'université nous a fait parvenir une photocopie de qualité inférieure.

La reproduction, même partielle, de cette microforme est soumise à la Loi canadienne sur le droit d'auteur, SRC 1970, c. C-30, et ses amendements subséquents.

Canada

Implementation of 3D External Photon Beam Dosimetry for the McGill Treatment Planning System

by

François DeBlois
Medical Physics Unit
McGill University, Montréal
March, 1996

A Thesis Submitted to the Faculty of Graduate Studies and Research in Partial Fulfillment of the Requirements for the Degree of Master of Science in Medical Radiation Physics

National Library
of Canada

Acquisitions and
Bibliographic Services Branch

395 Wellington Street
Ottawa, Ontario
K1A 0N4

Bibliothèque nationale
du Canada

Direction des acquisitions et
des services bibliographiques

395, rue Wellington
Ottawa (Ontario)
K1A 0N4

Your file Votre référence

Our file Notre référence

ISBN 0-612-12178-X

Canada

Abstract

A clinically-useful treatment planning system for external photon beam radiotherapy must yield fast and accurate calculations of the dose distribution in the patient. The interface of the system should be "user friendly" and designed to minimize user work and errors. Visualization of the patient volume and dose calculation results should provide necessary information without being confusing. A software module meeting these criteria has been implemented within the McGill Treatment Planning System (MPS). The MPS program is written in C code and compiled with CodeWarrior C\C++™ from MetroWerks Inc. The MPS program runs on the Apple Macintosh platform (either 68K or PowerPC series). This new software module permits dose calculation (modified Milan-Bentley method) and viewing of the patient volume in three dimensions. Patient anatomical data is acquired from computed tomography (CT) or magnetic resonance (MRI) images. The accuracy of the dose calculation has been verified through comparison of the calculated results with water tank and film measurements.

Résumé

Un programme efficace de planification de traitement par irradiation externe avec des photons doit permettre au dosimétriste de calculer de façon rapide et précise la dose dans le volume traité tout en lui offrant une interface agréable et performante tant au niveau de l'entrée des données que pour le visionnement du résultat des calculs et du volume du patient. Les bases d'un tel programme ont été implémentées pour le programme de planification de traitement "McGill Treatment Planning System" (MPS). Le programme MPS est écrit en langage C et compilé avec CodeWarrior C\C++™ de MetroWerks Inc. Il fonctionne sur plate-forme Apple Macintosh, séries 68K et PowerPC. Le système permet de calculer la dose (par méthode de Milan-Bentley modifiée) et de visualiser le volume du patient en trois dimensions. Les données anatomiques du patient sont obtenues par l'entremise de tomogrammes axials ou de coupes IRM. La précision des calculs du système a finalement été vérifiée en comparant les résultats calculés avec des mesures prises dans un réservoir d'eau et avec des films.

Acknowledgements

The research for this thesis was performed under the auspices of the Medical Physics Unit of McGill University, at the Department of Medical Physics of the Montreal General Hospital.

I am grateful and indebted to my research supervisor Dr. Conrado Pla for his guidance and patience during the course of my studies.

I also want to thank all my fellow students, in particular Arthur Curtin-Savard for his help with the use of the hospital treatment planning system, constructive criticism and valuable help in writing this manuscript. I am grateful to the professors and the clinical personnel at the Montreal General Hospital, in particular to Mr. Michael Evans for his help with the measurements. Finally, I thank my family and close friends for their love, friendship, and constant moral encouragement.

Table of Contents

Chapter 3

Chapter 4

Chapter 5

List of Figures

Chapter 1

Introduction

1.1 General Introduction

This chapter describes the basic characteristics of radiotherapy facilities and presents an overview of the radiotherapy treatment process in which treatment planning programs, the subject of this thesis work, occupy an important role.

1.2 Introduction to Radiotherapy

Radiotherapy is a treatment procedure that consists of imparting radiation to a diseased site with either cure or palliation as the goal. Radiation modalities certainly play a major role in the management of cancer since nearly half of today's cancer patients will receive radiotherapy as an important part of their treatment.

The radiation can be delivered to a diseased site in different ways. In *external beam radiotherapy*, the source of radiation is situated at roughly one meter from the patient. The radiation is incident on the patient from one or more collimated beams having selected field shapes (field size). The machines that produce the radiation beams are either linear accelerators or cobalt units. In *brachytherapy*, radiation is delivered to the diseased site by either intra-cavitary, interstitial or surface application. This takes the form of implants of radioactive seeds or ribbons. Photons and electrons, with energies in the kilo-electron-volt (keV) and mega-electron-volt (MeV) range are the types of radiation normally employed for radiotherapy procedures.

Different treatment strategies may be chosen when radiotherapy is used for the treatment of a lesion. In general, the typical procedure for treatments with external beams is as follows:

1) Treatment Simulation. For treatments that require little information on the patient anatomy, a normal simulator unit is used. This unit consists of a couch and a diagnostic x-ray tube mounted on a gantry that mimics the treatment unit setup. The patient is positioned on the treatment simulator and the physician with the help of the simulator output (film or fluoroscopy) decides the region to be treated, called the *target volume*. Reference marks are applied on the patient's skin to identify the center of the treatment fields. An axial contour of the patient is taken in the plane of the treatment with the help of a soft metal wire. Other contours at different levels may be taken if the variation in size of the patient across the field is important. Finally diagnostic x-ray films of the proposed treatment fields are produced as permanent records.

For cases that require more details of the patient anatomy, a CT scan is performed. The physician can then draw the target volume directly on the CT images. The contours of the patient in this case are obtained from the CT scans images information. The patient is either sent to the simulator for marking and obtention of the films or sent to the CT-Simulator to be virtually simulated and marked. The CT-Simulator is a CT linked to a computer that allows the physician to do the simulation through the computer interface by manipulating the CT images. "Virtual films" of any treatment field can be produced form the 3D CT data set.

During the simulation procedure, plaster casts, alpha-cradles, or orfits are fitted to the patient shape. These are used, as required, to obtain accurate and reproducible positioning of the patient.

2) Treatment planning. A treatment with external beams is usually composed of more than one beam, each beam having its own shape, size, energy, impinging angle and duration (weighting). All of these parameters vary from patient to patient. The optimal beam combination results in delivering a prescribed dose to the target volume and the minimum possible dose to surrounding healthy tissues. In modern radiotherapy, a computerized treatment planning system is used to find such an optimal combination. The patient contour, tumor (target volume) and structure information are sent to the dosimetrist who operates the computerized treatment planning system. By trying out several combinations of parameters and relying heavily on experience, the dosimetrist will find the best dose distributions achievable with the technology available in the

department. The ultimate goal of the treatment planning procedure is to produce a so-called treatment plan. This treatment plan will show *isodose lines*, or isosurfaces, connecting the points receiving equal doses, superimposed on the essential anatomical information of the patient in 2 or 3D. The treatment plan is then presented to the radiation oncologist who determines whether it is acceptable or not. If it is, the radiation oncologist decides on the dose prescription to be given to the diseased site in the patient.

3) Treatment delivery. A technologist then performs a calculation to translate the prescription dose to the machine setting for each daily treatment. If some fields are not rectangular or are intensity modulated by special shielding, blocks or attenuators are required and have to be constructed before the first treatment. The treatment is delivered in small daily doses of radiation (fractions of the total prescription), generally over a period of three to five weeks. Positioning of the patient is verified every few treatments with the help of portal films. The patient's condition is followed by weekly consultations.

4) Follow up. The condition of the patient is monitored by the physician for the coming years.

1.3 Historical Review of Computerized Treatment Planning:

Before the 1960's, treatment planning at a given plane in the patient was either performed by manual calculations of the dose at selected points in that plane or by matching the case at hand to a standard case for which the calculations were available in the form of 2-dimensional diagrams of the isodose distribution. These methods which relied on a very coarse description of the patient shape and composition were not precise enough to accurately evaluate the relative merit of different irradiation techniques. Obviously, a faster and more versatile way of doing treatment planning was desirable and this is why computers were introduced in this domain. The first use of computer for treatment planning is reported by Tsien in 1958 who used it to calculate the dose for rotational therapy treatments [TSIE]. Later, in the 1960's, Bentley developed a planning system which ran on a mainframe computer [BEN1]. These early systems of course had many drawbacks. Computers of the 1960's were very costly and required the use of punch cards, making the data entry tedious and subject to error. Futhermore, since the

calculation time of a distribution exceeded an hour, there was absolutely no possibility for an interactive use of the system.

A tremendous improvement in computerized treatment planning systems came in 1969 when Cunningham and Milan implemented a planning system on a mini-computer which had a simple user interface and connected peripherals. The system was later adapted by Bentley and Milan in 1971 [BEN2], [MILA]. Their calculation was performed in two dimensions in the plane of a patient axial cut and a distribution took less than five minutes to calculate for 1000 points on a uniform grid. Though still rather unsophisticated, the user interface was greatly improved compared to the mainframe systems, giving the user the capability of modifying the treatment parameters relatively easily.

The next important evolution in computerized treatment planning arose from improvements in diagnostic imaging tools, notably computerized tomography (CT) scanners [HOUN]. The axial cut images of a patient obtained from these scanners provided extremely valuable information on the patient anatomy that could be used directly for the treatment planning [GOI4]. Thus, in the early 1980's, General Electric Corp. commercialized *Target*, a computerized treatment planning system that used raster graphic display monitors displaying text menus and gray scale images acquired from the CT scanners. From then on, the successors to *Target* followed the same basic idea with different levels of sophistication in the user interface. Contouring objects such as patient's skin, tumor and other structures in the 2D image slice became a standard. The results of the dose calculation were then displayed as isodose lines superimposed on the CT images. These features are still commonly used in the current generation of treatment planning systems. However, the new generation of systems benifits from the ability to perform the dose calculation in a 3D volume, rather than a 2D slice plane of a given CT image. The former generation could not accomplish this, mainly due to computer calculation speed limitations. Some systems of that generation had capabilities for calculating dose in few parallel slices, but since their inherent calculation and geometry are still 2D, these systems are not true 3D system, and often called 2 1/2D. The limitations of these 2D based treatment planning programs are elaborated by Goitein [GOI3].

Since the variables involved in dose calculation problems are inherently 3D, a 3D based calculation technique is certainly preferable. 2D systems assume the patient surface to be the same throughout the patient. This assumption limits the dose calculation accuracy

especially when the patient profile varies rapidly in the direction perpendicular to the image cut plane. Also, treatments with non-coplanar beams are not possible. A 3D system does not suffer from these limitations and allows calculation of dose in arbitrary planes in the patient volume and even calculation in the entire 3D volume. This is a clear advantage of 3D systems, especially in treatments where critical organs have to be spared from radiation, the calculation of dose in the plane of that organ being very useful.

The viewing tools provided by a 2D system are also limited: the 3D visualisation of dose information is difficult or impossible. For 3D systems this information is readily available. The most recent systems, now use sophisticated 3D-based dose calculation algorithms [PCW3]. Other ones, such as the Peacock™ System (Nomos Corporation, Pen. USA) [CARO] are even starting to offer conformal treatment planning, which consists in optimizing conformity of the target volume to the treatment volume. They also have a more complete set of tools for 3D visualization of the patient data set such as beam eye's view (BEV) and observer's eye view (OEV) [GOI1], [GOI2] and [MOHA] (see also Chapter 4 for examples).

The characteristics of the treatment planning systems which continuously improve are the price, the user interface, and the calculation speed and complexity. These improvement are made possible mainly because of the constant improvement in computer technology. Obviously, the calculation speed and sophistication of these systems depends heavily on the power of the computer on which they run, which is related to the price of the system. At the present time, the commercial treatment planning systems are developed principally for UNIX-based workstations which are very expensive and often cumbersome to use. Fortunately, it is becoming possible to produce high quality treatment planning systems also on personal computers. These are far less expensive (~10×) and generally more friendly to use. The *McGill Treatment Planning System* written by Dr. Conrado Pla at McGill University, has been developed for standard Apple Macintosh computers. So far, the *McGill Treatment Planning System* provides brachytherapy and stereotactic treatment planning utilities [PLA1]. However, to fully cover the treatment planning needs of a radiotherapy department, external beam treatment planning for photons and electrons must be incorporated.

1.4 Aims of this work

The need for external photon beam treatment planning capabilities in the *McGill Treatment Planning System* motivates this thesis work. The specific goals of the project were the following: 1) to implement the basic algorithms for external beam planning based on measured beam parameters methods 2) to make these algorithms fast enough to be used interactively (this mainly implied speeding up the algorithms for 3-D depth search which are essential to this type of dose calculation method) and finally, 3) to implement some 3D visualization tools for viewing the patient volume, particularly an observer view display.

1.5 Thesis Organization

Chapter 2 covers the basics of external photon beam treatment planning by describing the treatment variables and the physics required for the planning and will go through some details on the dose calculation algorithms. Chapter 3 will describe the material and methods used for the implementation of the algorithms. Chapter 4 describes the verification procedures that were performed to verify the accuracy and reliability of the program (system verification). Finally the conclusion will summarize what was implemented and the limitations of the program.

Chapter 2

Theory of External Beam Treatment Planning

2.1 Introduction

Before a radiotherapy treatment can take place in the clinic, the precise setup for the treatment has to be determined from the physical geometry of the patient, the physician prescriptions, and the treatment modalities that are available. This planning process is called treatment planning. As stated in Chapter 1, the focus of this thesis will be on treatment planning for external photon beam treatments.

Normally, the physician prescription consists of a dose value to be delivered to the target volume of the patient. It also includes, if necessary, dose limits to critical organs that could be affected deleteriously if they were to receive a higher dose. The physician is also responsible for delineating the tumors and other critical organs. The physical geometry of the patient is very complex and specific to every single patient. This information is obtained by axial scanner images acquired by different imaging modalities such as CT or MRI scanners. The choice of the treatment modality, will vary with the availability of particular treatment units at the clinic and the type of disease. The treatment modality determines the type and properties of the radiation employed for the treatment. The treatment is usually composed of one or many external beams of various field sizes and impinging angles, particle type (generally photon or electrons) and beam energy. Dosimetrist (or physicist) will try to select these parameters such that the target volume will receive an accurate, precise and uniform radiation dose and that the surrounding healthy tissue (and critical organs) receive as low a dose as possible.

Certain tools facilitate this complex task. The treatment planning system simulates the results of different treatment techniques. The clinical requirements suggest that the computed dose has to be accurate within 2% [ICR2]. The selected final plan, when approved by the physician, is an official permanent record illustrating how the treatment was intended to be delivered.

Before discussing the means of implementation of a treatment planning system, a formalism for dosimetric calculations has to be defined to describe the physics of dose deposition in the treated volumes. Only the parameters and factors that are required for

the comprehension of the thesis work will be presented, for a more complete discussion the reader can refer to [JOCU] or [KHAN].

2.2 Treatment Setups

Before discussing the physics of the dose deposition and means of calculating the dose in the patient volume, it is important to describe the treatment environment and the setups that are used in external beam radiotherapy.

The patient is positioned on a couch which can be rotated around a single axis (angle ϕ), (cf. Fig. 2.1). The couch can also be moved in space for a convenient positioning. In the case of external photon beam treatment, the radiation beam is provided by a linear accelerator or a cobalt-60 machine, both machines having the same couch/gantry movement capabilities. The gantry can be rotated around a single axis (angle θ). The size of the beam is defined by the opening of the collimators in the gantry head. These collimators can also be rotated around a single axis, (angle δ).

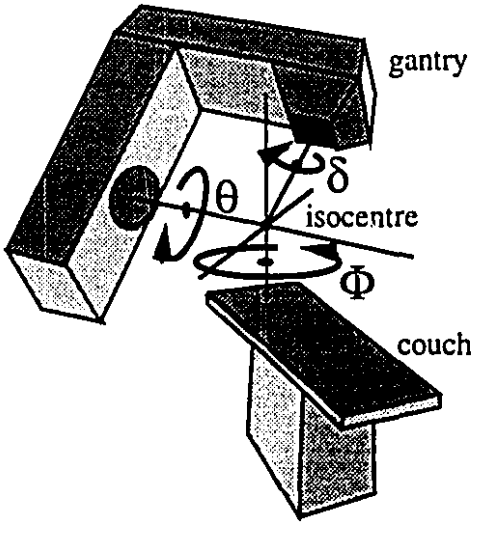

Figure 2.1. The treatment environment

The isocentre location is important when specifying the treatment since it is the common point along the axis of rotation of the gantry, the collimators, and the couch and therefore remains fixed in space. The couch can also be moved vertically and laterally so as to position the isocentre at the desired location in the patient volume.

There are two principal setups or arrangements for external beam treatments: source to skin distance (SSD) setup and source to axis (SAD) setup. Figure 2.2 illustrates graphically the differences between the two.

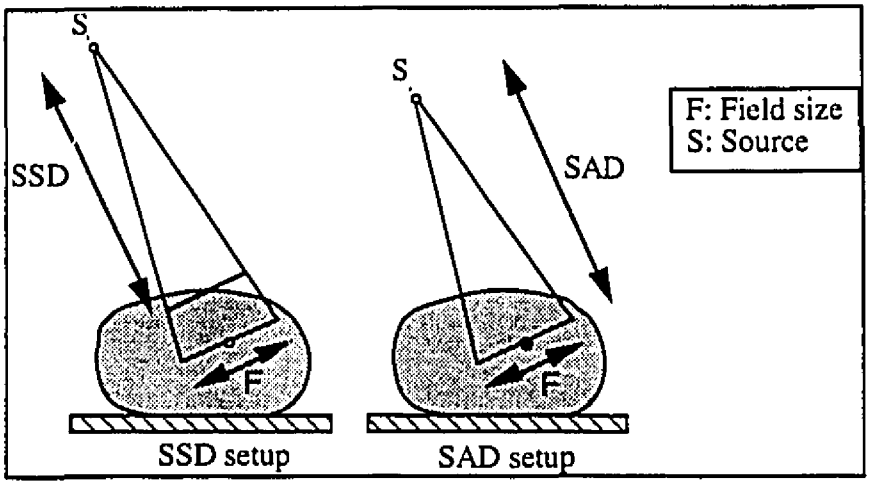

Figure 2.2. Difference between SSD and SAD treatment setups.

Each machine has a specific SAD distance which corresponds to the distance between the source position and the isocentre. This distance is usually 100 or 80 cm. For an SSD setup, the patient is placed such that the isocentre is situated on the patient surface. The field size is then specified at this level. For an SAD setup the isocentre is within the patient and the field size is defined at the isocentre. One difference between the two setups is that in the SAD setup the patient is closer to the source of radiation, and therefore, the isodose distributions resulting from these two setups are somewhat different. The tumor dose will be greater with the SAD setup than with the SSD set-up for the same amount of radiation given from the source. For SAD and SSD treatment beams that have the same surface field size, the geometrical beam divergence will be slightly greater for the SAD setup.

The SAD setup is generally more practical to use for treatment techniques which use multiple beams because the patient does not have to be repositioned for every beam since the SSD distance does not have to be constant.

2.3 Deposition of dose

Interaction of the radiation with the medium will result in a transfer of energy to the medium. The *dose* is a quantity corresponding to the amount of energy deposited per unit mass. The units of dose are the Gray (Gy) where 1 Gy corresponds to 1 Joule per kilogram (J/kg). Radiation is generally classified in two types: directly or indirectly ionizing, depending on whether the primary source of radiation consists of charged or uncharged particles.

In the case of non-ionizing particles such as photons, these must first interact with the medium, according to some probability distributions. Many different interaction processes are possible within the clinical treatment energy range. The three main interactions are: photoelectric effect, Compton scattering, and pair production. Figure 2.3 shows the different "zones" where these types of interactions are dominant as a function of the atomic number of the medium versus the photon beam radiation energy.

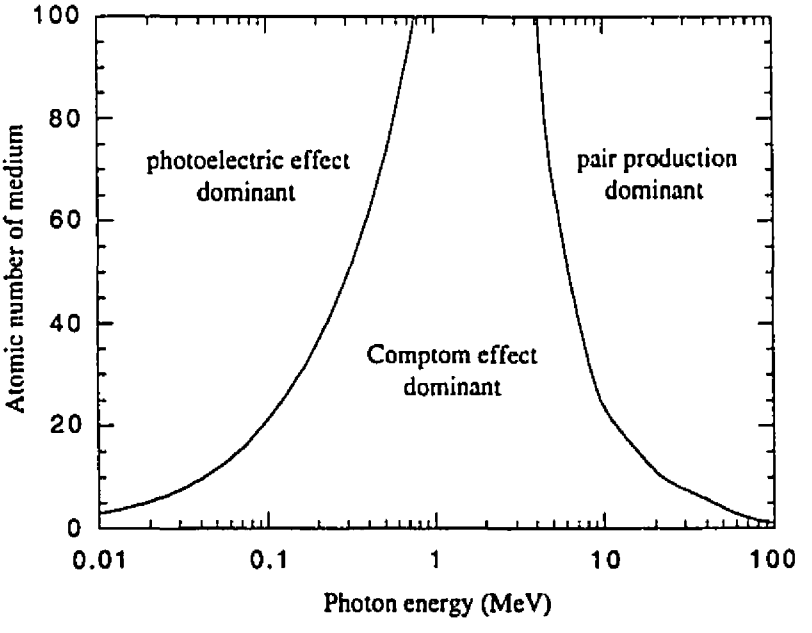

Figure 2.3. Zones of dominant interaction type with respect to the photon energy and the atomic number of the medium. [EVAN]

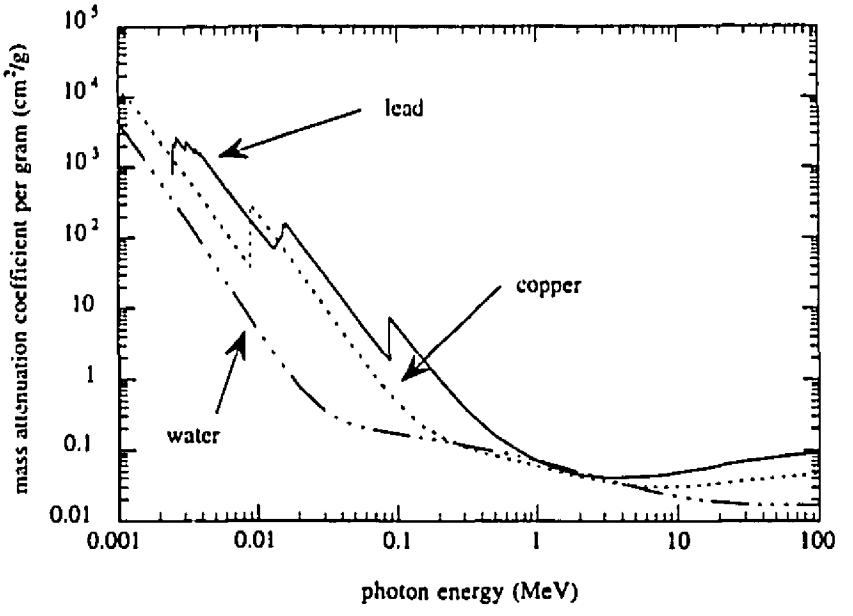

Figure 2.4. Mass attenuation cross sections for the sum of the interaction processes as a function of energy in various materials.

The total probability of interaction is often illustrated as by the mass attenuation cross section, Fig. 2.4. The abrupt changes in the curves correspond to the photo-electric absorption edges at certain energy values for various materials.

The result of these photon interactions within the medium is that some electrons (or positrons) are set into motion within the medium. These first interactions are giving rise to the KERMA (Kinetic Energy Release in the Medium) (Fig. 2.6), that represents the rate of transfered energy to medium per unit mass of medium. The units of the KERMA (J/kg) are the same as for *absorbed dose*, the energy that is absorbed per unit mass of the medium. The KERMA is maximum at the surface and goes down with depth since it is proportional to the photon fluence that also decreases with depth. These high energy electrons transfer their kinetic energy to the medium through soft and hard collisions or through radiation (Bremsstrahlung) at various distances from their creation point. Since the dose is approximately proportional to the electron fluence, it will increase with depth to reach a maximum at depth d_{max} since at the surface there are few electrons set in motion, and a maximum will occur where electrons that were set in motion near the

surface deposit their energy; the region between the surface and d_{max} is referrred to as the *build up region*. At depths further than d_{max} the dose goes down because of exponential attenuation of the photon fluence. An *electronic equilibrium* is reached at d_{max}. The electronic equilibrium means if one looks in a slab of material perpendicular to the direction of the incident photons, the number of electrons that are going in that slab is equal to the number of electron going out.

The linear rate at which the electrons lose their energy in the medium, divided by the density of the medium is called the mass stopping power (S), Fig. 2.5, and is either collisional or radiative. These collisional interactions either ionize or excite the atoms of the medium which may result in breaking molecular bounds or producing heat and as a consequence some cells will lose their reproductive capabilities through the alteration of their DNA molecules.

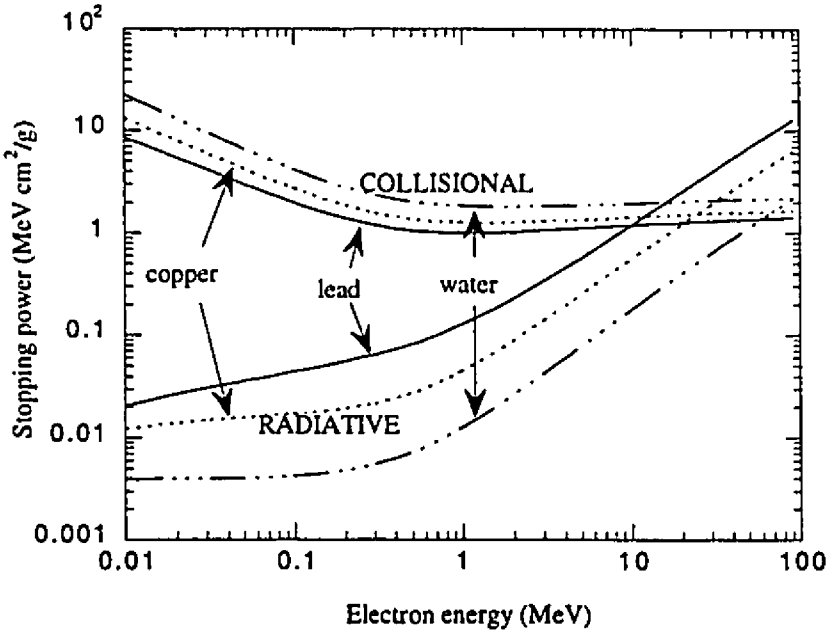

Figure 2.5. Mass collisional and radiative Stopping Power S as a function of energy

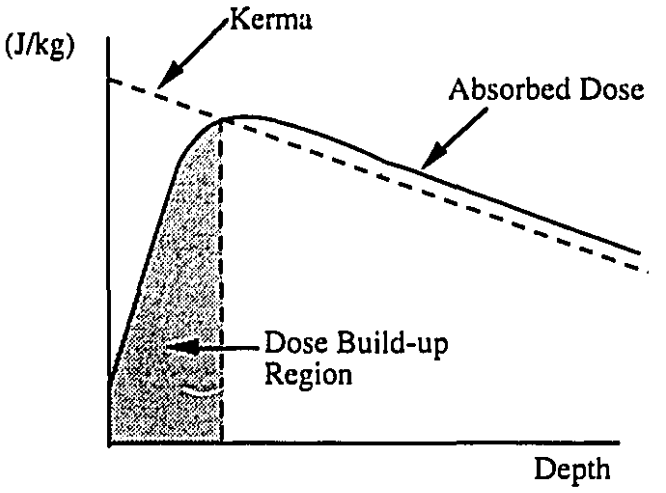

Figure 2.6. Kerma vs. Absorbed dose

Fig. 2.10 shows that the build up region increases with the energy of the incoming photon beam so that the depth at which the dose is maximum becomes deeper. This effect is often useful for treatment in which a sparing of the subcutaneous healthy tissues is desired. This is called skin sparing effect.

The principal difficulty when dealing with the calculation of the absorbed dose in a patient volume comes from the fact that the dose at each particular point of the volume depends on all parts of all of the irradiated volume. For instance, in Fig. 2.7 the dose at point P has a contribution from the primary radiation that comes directly along the primary ray path but it also has a contribution from the radiation scattered once at angle θ within the volume element dV. This scattered contribution has to be integrated over all the volume elements dV of the entire volume also over all possible scattering angles θ and finally over all multiple scattered photons since some radiation scattered in all other volume elements dV could also come from other scattering events (single or multiple).

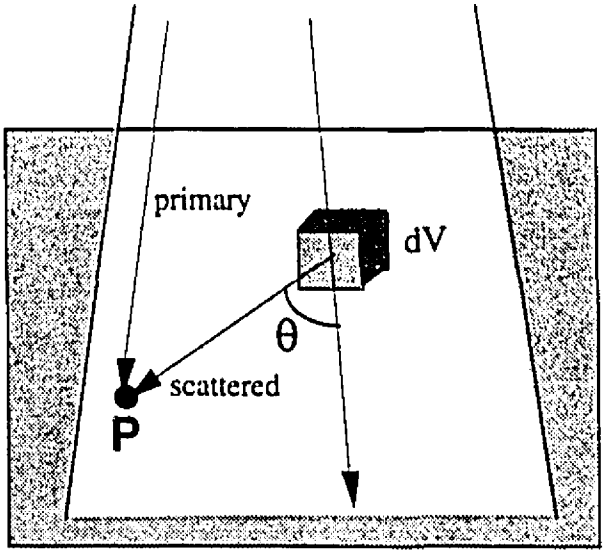

Figure 2.7. Contribution to the dose at point P from primary and scattered radiation.

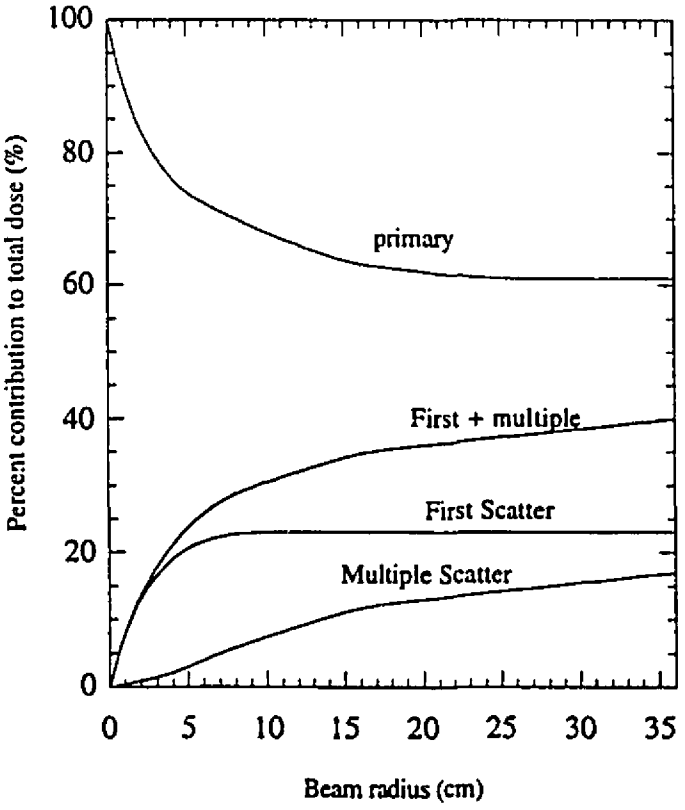

Figure 2.8. Percent contribution to the total dose at a depth of 10 cm in a water phantom from a Cobalt-60 radiation source. [CUN0]

The relative contribution of primary, first and multiple scatter as a function of field size for cobalt-60 radiation at a depth of 10 cm in a water phantom is illustrated in Fig. 2.8. One can note that the proportion of scatter radiation for field sizes greater than 20×20 cm^2 is greater than 1/3 of the total dose.

Moreover, the cross sections vary with the composition (electron density) of the treated volume material (cf. Fig. 2.4). This will produce sudden changes in the electron fluence within the treated patient volume (e.g. tissue vs. bone or lung) which itself has a complex 3D geometry, curved surfaces and interfaces.

Finally, a radiation treatment beam is not monoenergetic: it is composed of particles that have a spectrum of energy.

Because of all these reasons, the problem of absorbed dose calculation at any point is extremely difficult and there is no exact analytical solution available.

2.4 Dose calculation algorithms

The dose calculation algorithms currently employed for radiotherapy treatment planning are generally classified in three categories: Monte Carlo method, convolution algorithm methods and empirical methods.

2.4.1 Monte Carlo method

The Monte Carlo technique is the most general and rigorous method because it solves the problem of radiation transport by physically simulating the deposition of dose in the 3-dimensional volume of the patient [ANDR]. Primary particles as well as the scattered radiation particles are followed. The dose contribution due to charged particle tracks crossing the volume of interest is summed. For this iterative method to converge to a precise solution 1 million to 10 million particle histories are required[CUN1]. Therefore the main impediment to the clinical use of this method is the computational speed: a typical patient demands many hours of processor time even on today's powerful

workstations. Another drawback is that the method requires a precise knowledge of the angular energy cross section of the particles, which is not accurately known. For these reasons Monte Carlo is not currently used in routine clinical treatment planning, where fast calculation of dose is required. However, the Monte Carlo technique is an essential simulation tool to provide starting data for other methods or to test the results of other methods(e.g., convolution algorithms). Monte Carlo will continue to be used in the future to verify the results of these methods especially where particularly complex geometry limits the calculation accuracy of these other methods.

2.4.2 Convolution algorithm methods

These algorithms are based on the fact that the primary and scattered radiation contributions to the absorbed dose can be treated separately. Defining a source function p(x, y, z) that corresponds to the photon fluence incident on a volume element dV at location (x, y, z) of the irradiated volume, and an energy spreading term or scatter function s(x, x' ; y, y' ; z, z') that corresponds to the energy set in motion in a volume element dV' at (x', y', z') that further reaches dV, the dose at (x, y, z) is given by the superposition of the two functions for all scattering elements of the treated volume, i.e.,

$$D(x,y,z) = \int_V p(x',y',z') \cdot s(x,x';y,y';z,z')dx'dy'dz' \qquad (2.1)$$

In principle the "s" function, often called *kernel* or dose spread function (DSF), can include all multiple scattered radiation from any type of interaction. However the DSF in an inhomogeneous medium with a divergent polyenergetic beam changes at every particular location of the volume element dV. The integrals of the DSF can be measured as the Tissue Air Ratio (TAR), and the Scatter Air Ratio (SAR) (cf. Section 2.5). A numerical differentiation of these quantities yields the DSF, (also called differential SAR or dSAR). The DSF can also be obtained through Monte Carlo methods [MACK]. For non-divergent monoenergetic beams impinging on an homogeneous medium the DSF is invariant and s becomes s(x-x'; y-y'; z-z') (a simple function of the relative position of dV and point (x, y, z)) and Eq. 2.1 becomes a simple convolution. The existing algorithms use equations of the form of Eq. 2.1 except that the p term is extracted from the integral and solved separately. Various possible convolution and superposition algorithms such as convolution with a 1-D kernel, convolution in 2-D using a pencil kernel, superposition in 3-D using a point kernel have been implemented [CUN1]. The calculation speed of these

algorithms is still limited (couple of minutes per treatment beam) and thus not generally clinically applicable.

Many "semi-empirical" algorithms such as the Equivalent TAR [SONT] and the Delta Volume algorithm [WON1] are special cases of the convolution algorithm method.

2.4.3 Empirical methods

Empirical methods are the oldest and most widely used techniques to calculate the absorbed dose in the patient volume. These methods rely on measured data. The technique was first employed to perform manual treatment planning. An isodose distribution is measured for a specific beam, under ideal conditions, i.e. in a homogeneous water square box phantom that mimics a semi-infinite volume of water. Water closely approximates the radiation absorption and scattering properties of muscle and other soft tissues and since it is cheap, easy to work with and universally available it is the most widely used tissue substitute. The required data is measured for a collection of beams of various field sizes and modifiers that is representative of the machine capabilities. The isodose distribution corresponding to the desired treatment beam is superimposed on the patient cross section and the isodose line or the dose at selected points within that patient slice can be calculated approximately by correcting for the patient curvature, non-normal (oblique) incidence and inhomogeneity differences between the two irradiated volumes. This method was later extended to computer usage by digitally storing the beam information in computer memory [BEN1]. The accuracy of the calculation depends heavily on the correction methods that are used to map the dose measured in the ideal geometry to the dose generated in the patient geometry. These corrections methods are elaborated in many textbooks [JOCU], [KHAN], [BEN0].

The dose calculation algorithms implemented for this thesis work are based on the empirical method. This technique was chosen mainly for considerations of calculation speed. The next section describes some quantities, either measured or derived from the simple dose measurements, that are important to understand the inputs for the implementation of our treatment planning program.

2.5 Measured parameters

2.5.1 Percent depth dose

As a beam of high energy photons impinges on some material it transfers some of its energy to absorbed dose in the medium. Figure 2.10 shows how dose typically varies with depth along the central axis of the beam. The depth at which the dose is maximum is called d_{max}. When the dose values are normalize to 100% at depth d_{max}, the quantity is called *percent depth dose* (PDD).

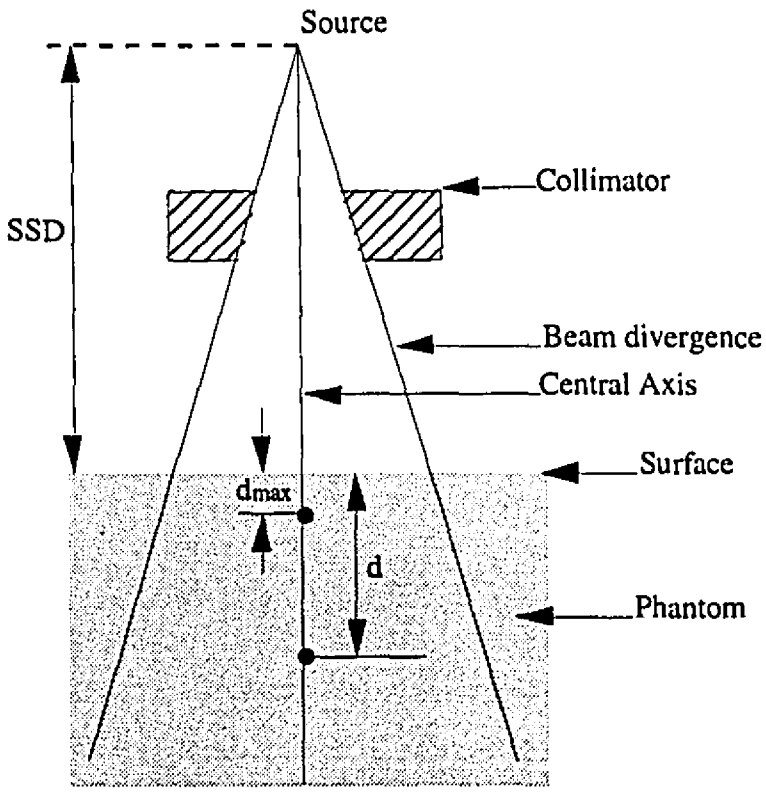

Figure 2.9. Experimental setup for the measurement of PDD values.

The percent depth dose, Eq.2.2, is used with the SSD setup to relate the dose (D) at a given depth (d) to the dose at depth of maximum dose (d_{max}) on the central axis of the beam.

$$PDD(d,A,SSD,E)=\frac{D(d,A,SSD,E)}{D(d_{max},A,SSD,E)}\cdot 100 \qquad (2.2)$$

The percent depth dose is a function of depth (d), field size at phantom surface (A), source to surface distance (SSD), and energy (E) of the radiation beam, (cf. Fig. 2.10). There are two important parts in a PDD curve: the *build-up region* which extend from the surface to d_{max} and the *fall-off region* from d_{max} to the deepest measured depth. Note that as the energy of the beam increases the value of d_{max} increases which is also illustrated in Fig. 2.10.

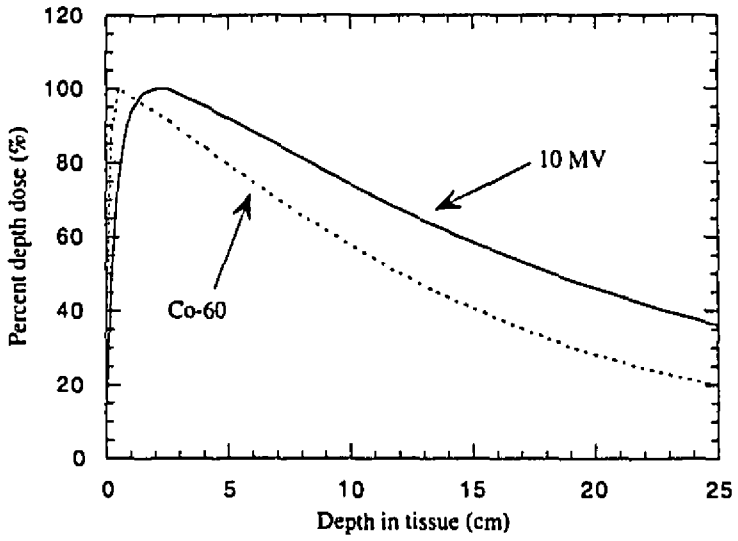

Figure 2.10. Typical percent depth dose curves for a 10 × 10 cm^2 field for a Cobalt-60 (T-780) machine and Clinac-18 10 MV linear accelerator.

2.5.2 Tissue Air Ratio, Tissue Phantom Ratio.

The *Tissue to Air Ratio* (TAR) quantity is used with the SAD setup to simplify the calculations. TAR is the ratio that relates the dose to a small mass of medium in air D_q', to the dose D_q at a particular depth d in the medium at the same SAD distance, (cf. Eq. 2.3).

$$TAR(d, A_q, E) = \frac{D_q(d, A_q, E)}{D_q'(SAD, A_q, E)} \tag{2.3}$$

d is the depth of the point in medium, A_q is the field size at that depth and E is the energy. There is one major problem with the use of TAR. The measurement of D_q' is dependent on a precise in air measurement, which is not practical at photon energies

higher than 3 MeV. Thus at higher energies it is necessary to take the reference dose measurement in phantom rather than in air. This is why the *Tissue Phantom Ratio* (TPR) was defined. It is the ratio of the dose at a certain depth d to the dose at a reference depth d_{ref} for the same SAD and field sizes A_q at both points, cf. Eq. 2.4.

$$TPR(d, d_{ref}, A_q, E) = \frac{D_q(d, A_q, SAD, E)}{D_q(d_{ref}, A_q, SAD, E)} \tag{2.4}$$

The *tissue maximum ratio* (TMR) is the particular TPR where the reference depth is taken at the d_{max} value of the beam.

TPR and TAR are related as :

$$TPR(d, d_{ref}, A_q, E) = \frac{TAR(d, A_q, E)}{TAR(d_{ref}, A_q, E)} \tag{2.5}$$

TAR, TPR and TMR can also be shown to be independent of the SAD (cf. [KHAN]).

2.5.3 Beam profiles

The previous quantities relate and describe the relative dose values between points along the central axis of the beam. However, to do treatment planning, a means of estimating the dose at *any* location inside the patient volume is needed. The *Off-Axis Ratio* (OAR) or *beam profile* relates the dose on the central axis to the dose at an off-axis perpendicular distance (Eq. 2.6). The OAR is a function of depth and off axis distance. In general this function is really a three dimensional function: position (x, y) in a plane perpendicular to the beam at depth d in phantom.

$$OAR(d, x, y) = \frac{D(d, x, y)}{D(d, 0, 0)} \tag{2.6}$$

The profile is not perfectly flat at every depth, i.e., flat from the center to the edge of the field, before the fall off region, (cf. Fig. 2.11). This is due to two factors. Firstly, the dose given to the points on the edge of the field is produced by photons that have traveled a greater distance than the photons at the center of the field. The *inverse square law*

states that the intensity of photons falling on a flat surface from a point source is inversely proportional to the square of the distance from the point source. The points at the edges of the fields will therefore receive less dose than the center points. Secondly, the radiation source itself has to be well understood. When photon radiation is produced by a linac, a flattening filter is present. This flattening filter will influence the mean effective energy across the field. The photons in the central beam region have traversed a thicker portion of the filter than the photons at the edges. Therefore these central photons will have a higher mean energy compared to the ones at edge, producing a faster fall off of the dose at the edges than at the center since lower energy photons are less penetrating (cf. Fig.2.12A). Most linacs used for radiotherapy have a flattening filter designed to deliver a "flat" dose profile at a depth of 10 cm, which is a typical treatment depth. This results in slight overdosing ("horns") at the edges of the field at depths shallower than 10 cm (cf. Fig. 2.12B) . Profiles of cobalt-60 beams will look very similar to linac beams' profiles (Fig. 2.11). The range of cobalt-60 source sizes varies from 2 to 7 cm^2 diameter. Linacs have an equivalent source size of about 2 mm^2. The large source size of a Co-60 source will create a larger penumbra, thereby smoothing out the beam edges to a greater extent. On the other hand, the flattening filter of the linac creates a lot of scatter that will smooth the beam edges so that the dose profile becomes similar to Cobalt-60. Finally, since all treatment beams are divergent (to some extent) the dose profiles will broaden with depth.

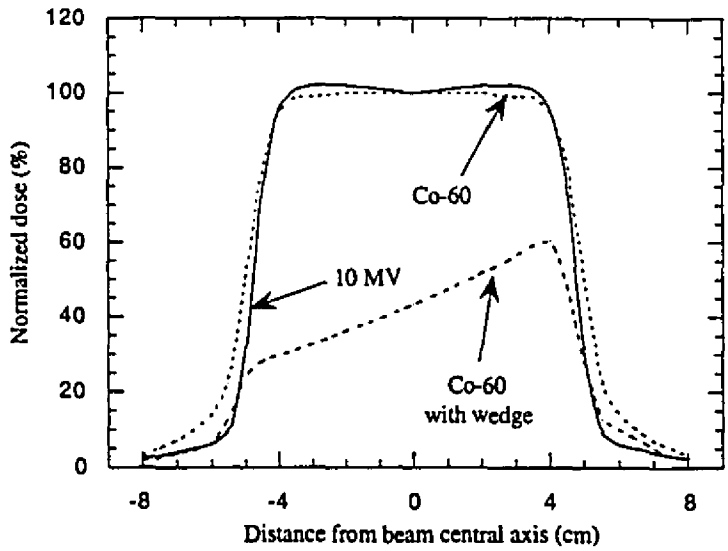

Figure 2.11. Off-axis ratio for a 10 × 10 cm^2 field for a cobalt unit and a Clinac-18 linear accelerator. The third curve illustrate the effect of a wedge on the dose profile (cf. Section 2.6).

A method to obtain a beam with a narrow penumbra (sharp dose fall off) is the so-called "half-block" technique (Fig. 2.12). In this method, a thick piece of lead with a straight edge is placed along the central axis of the beam to block exactly half of it. Since this "newly" created edge of the beam is at the center of the beam, there is very little divergence and therefore almost no penumbra.

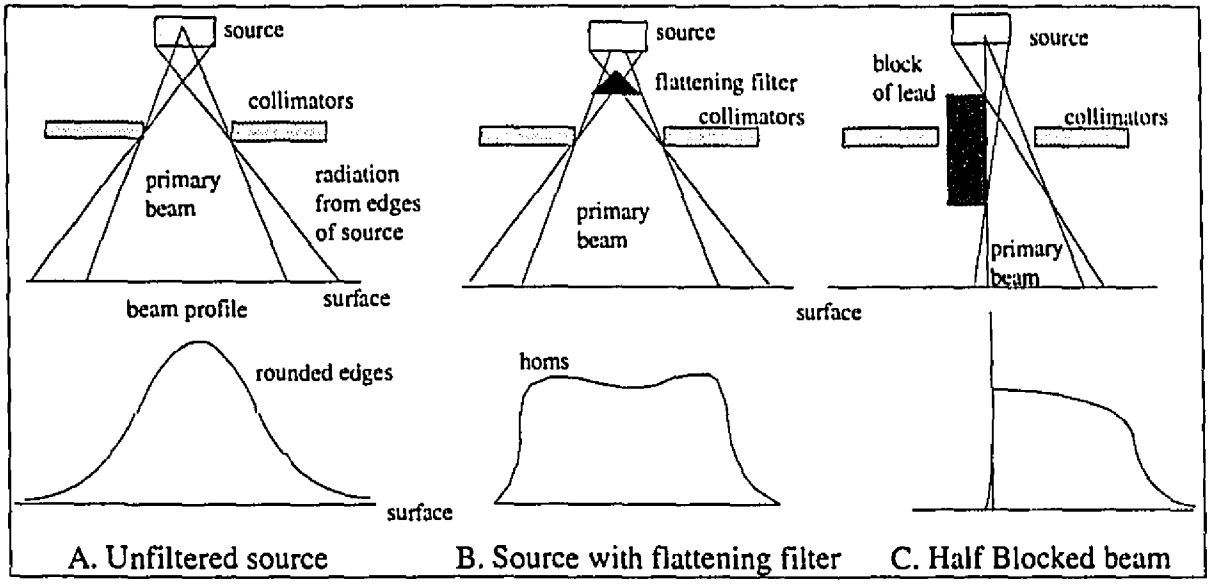

Figure 2.12. Appearance of typical dose profiles for various setups.

2.5.4 Scatter Related Parameters

As mentioned previously, the scattered radiation contribution to the dose is important. Some functions describing the scatter component of radiation therefore have to be introduced.

Peak Scatter Factor (PSF)

The *Peak Scatter Factor* is defined as the ratio of the dose at d_{max} in phantom to the dose at the same point in air for an SAD setup, (cf. Eq. 2.7). It is a function of the field size A and the energy E of the radiation beam.

$$PSF(A,E) = \frac{D_p(A,E)}{D'_p(A,E)} = TAR(d_{max}, A, E) \tag{2.7}$$

Scatter-Air Ratio (SAR)

This *Scatter-Air Ratio* is used to calculate the scatter contribution to the dose in the medium. It is particularly useful for the dosimetry of irregular fields, i.e. fields that are not rectangular, when one has only access to tabulated values of regular field data. It is also useful whenever one needs to separate the primary and scatter contribution components. The scatter-air ratio is defined as the ratio of the scattered dose at a given point in the phantom to the dose in free space at the same point. It only depends on beam energy, depth, and field size. A common way of expressing it is by a difference of TAR, (cf. Eq. 2.8) since the scattered dose at a point cannot be measured but is given by the difference between the total dose at a point and the primary dose at the point. The TAR for the zero area field size theoretically represents the primary component of the beam since no scatter radiation is produced in the phantom thus,

$$SAR(d,A,E) = TAR(d,A,E) - TAR(d,0,E) \tag{2.8}$$

Where $TAR(d,0,E) = e^{-\bar{\mu}(E)(d-d_{max})}$ where $\bar{\mu}(E)$ is the average linear attenuation coefficient for the beam.

Collimator Factor (CF)

The *Collimator Factor* accounts for the change in dose due to the variation of scatter produced in the head (collimator assembly and filters) of the treatment machine at different field sizes. It does not account for the change of dose resulting from variation of scatter in the medium at different field sizes. By definition, the collimator factor is normalized to a field size of 10×10 cm^2. So CF(A) = 1 for A= 10 cm, side of the square field size.

At a given energy the collimator factor (CF) is only dependent on the treatment field size. It is the ratio of the dose to a small mass of medium in air for a field size A (length of one side of a square field) to the dose in air to a small mass of medium for a field size 10×10 cm^2,

$$CF(A,E) = \frac{D'_p(A,E)}{D'_p(10,E)} \tag{2.9}$$

The collimator factor is measured in air at the SAD (source to axis distance) of the given machine.

Relative Dose Factor (RDF)

The *Relative Dose Factor* is used to account for the increase in dose due to both the scatter created in the treatment head of the machine and the scatter created in the medium as the field size is increased. It relates the dose at d_{max} in the medium for different field sizes measured at the typical source to surface distance (SSD) of the machine, (Eq. 2.10). Again this factor is normalized to a $10 \times 10\ cm^2$ field. Here again this factor is only a function of the field size A and of the beam energy E.

$$RDF(A,E) = \frac{D_p(A,E)}{D_p(10,E)} \tag{2.10}$$

Scatter Factor (SF)

The scatter factor cannot be measured but is used to relate the CF to the RDF. The SF takes into account the increased dose in the medium from increased scatter in the medium. SF is also measured at SSD. For a given energy, the SF only depends on field size A and energy E, Eq. 2.11.

$$RDF(A,E) = \frac{D_p(A,E)}{D_p(10,E)} = \frac{D'_p(A,E)}{D'_p(10,E)} \cdot \frac{PSF(A,E)}{PSF(10,E)} = CF(A,E) \cdot SF(A,E)$$

thus we can also write: (2.11)

$$\mathrm{SF(A,E)} = \frac{RDF(A,E)}{CF(A,E)} = \frac{PSF(A,E)}{PSF(10,E)} \frac{D'_p(A,E)}{D'_p(10,E)} \frac{1}{CF(A,E)}$$

2.6 Beam Modifiers and Isodose Curves

Once the dose values at any point in a treated plane are known, lines connecting together points that receive the same dose can be drawn. These lines are called *isodose lines*. In a volume, a similar exercise will produce *isodose surfaces*. Figure (4.3) shows isodose lines calculated with the *McGill Treatment Planning Program*. The isodose curves obtained through calculation of the dose in the patient image plane are shown superimposed on top of the image. This is a standard way of presenting the dose calculation results for a treatment plan.

It is often necessary to alter the shape of the isodose distribution in the patient by introducing a wedge filter in the beam. The function of a wedge is to attenuate the beam to varying degrees across its width. The attenuation increases with decreasing photon energy (for photon energies lower than ~ 3 MeV in lead) and it also increases with increasing photon energy (energy higher than ~ 3 MeV) in lead, therefore a photon beam of poly-energetic radiation could experience "hardening" or "softening", respectively, depending on its energy. In the case of hardening, (which is the case for most treatment beams), the beam emerging from the wedge, although having lower intensity, should be more penetrating than the open beam, thereby modifying slightly the PDD curve.

Two parameters are needed to characterize a wedge: the *Wedge Factor* (WF) and the *Wedge Angle*. The wedge factor is given by Eq. 2.12,

$$WF = \frac{D_{\max}^{wedge}}{D_{\max}^{no-wedge}} \tag{2.12}$$

The wedge factor relates the output of the machine with the wedge in place to that of the open beam at d_{max} for a $10 \times 10\ cm^2$ field.

The wedge angle is defined as the angle of the 50 % isodose line with the normal to the central axis of the beam. For example a 45° wedge produces an isodose distribution in which the 50% isodose line makes an angle of 45° with the normal to the central axis. An example of a wedged beam profile is shown in Fig. 2.11. Dynamic wedges, produced by a dynamic collimation of the beam are now starting to be available. They are computer controlled and give more wedge angle possibilities with no physical manipulation.

Other beam modifiers such as blocks or compensators may be used. Compensators, usually made of varying thickness of a heavy metal, will modulate the intensity of the field irregularly to obtain a better uniformity of the dose to the target volume. Blocks are used to change the shape of the field from the usual rectangular shape or to have a sharp fall off of the dose at the edges of the field as shown in Fig. 2.12C.

The isodose distribution is also dependent on the energy of the treatment machine. As the energy is increased, the penetration increases. Also, the higher the energy is, the more forward peaked is its scatter radiation. This implies that a higher energy beam is not only more penetrating, but also that its beam profile at any depth is more uniform and better localized than a low energy beam. Another important factor is the size of the radiation source.

Treating from the plan

The isodose lines of the treatment plan represent relative values. For a SSD setup, the distribution is often normalized to 100% at depth d_{max} on the central axis of the beam. For the SAD setup, the distribution is often normalized to 100% at the isocentre point. From the plan, the general method to find the time, for a cobalt-60 machine, (or the number of monitor units for a linear accelerator) required to deliver a certain tumor dose is given by Eq 2.13:

$$(T(\text{min})\ or\ MU) = \frac{TD(cGy)\cdot W}{RDV\cdot DR'} + [shutter\ \ error] \qquad (2.13)$$

where

- TD is the tumor dose in cGy
- W is the weighting for the calculated beam
- RDV is the relative dose value at the prescribed point from the plan
- DR' is the dose rate in phantom for a reference field size (in cGy/min for cobalt-60 or in cGy/MU for a linac); this quantity is measured for the particular treatment machine.
- The ratio TD/RDV is called the given dose GD.
- The shutter error is typically in 1/100 of a minute and only applies for a cobalt-60 machine, and is caused by finite opening and closing time of the shutter mechanism.

2.7 Standard corrections for empirical methods

The empirical methods use parameters measured in ideal conditions, as discussed previously, and then apply a correction to the ideal dose distribution to determine the dose distribution in the patient volume. The two factors for which one has to correct are the oblique incidence of the beam (or equivalently curvature of the patient surface) and the non-homogeneity of the treated volume. Under ideal conditions, when measuring various parameters such as PDD and beam profiles, the electronic equilibrium condition for kerma ≡ dose is satisfied. However in a typical patient volume some heterogeneous structures may have a density considerably different than water (ρ=1.00g/cm^3), for examples lungs ($\rho \approx 0.3$ g/cm^3) and bones ($\rho \approx 1.6$ g/cm^3). As pointed out in Section 2.3, the dose deposition will vary considerably near interfaces of structures that have a different density. These two differences (oblique incidence and heterogeneous structures) between ideal conditions and patient volume are used to modify the measured parameters in order to approximate the dose delivered to the patient. The usual approach is to find the *radiological* or *equivalent path length* (RPL or EPL) at every point of calculation. The RPL is a corrected slant depth (along the ray line) scaled according to electron density along the path, water density being normalized to a density of 1. The basic assumption of these models is that the correction to the dose at a point is only dependent on the tissues lying on the path of the ray.

The basic measured parameters are usually percent depth dose and off-axis ratio defined in Section 2.4. This section summarizes some correction techniques that are used. Then the method that was implemented will be described in detail.

2.7.1 Contour irregularities corrections

These corrections are applied when the surface of the patient is curved or when the beam is obliquely incident on the surface. In general, these type of corrections are applicable for an incident angle up to 45° for beam energies higher than 1 MeV and up to 30° for orthovoltage beams [KHAN]. Some manual calculation methods such as the isodose shift method (that are crude approximations) will not be discussed here, cf. [KHAN] or [JOCU] for more details.

Effective SSD method

This method consists in sliding the isodose lines with respect to the corresponding point of calculation and correcting for the inverse square law. Figure 2.13, illustrates the situation for an SSD setup with a field size A at the surface. The corrected dose at point Q will be given by Eq. 2.14. The effective SSD correction is frequently used in computerized treatment planning.

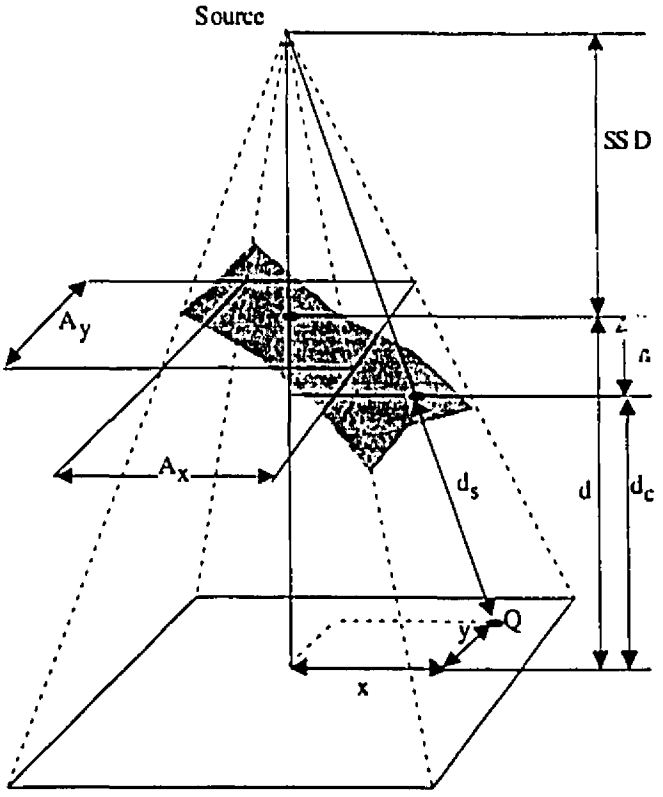

Figure 2.13. Set-up to illustrate the geometry of the dose calculation parameters when the calculation point is Q.

$$D(x,y,d) = D(d_{max}) \cdot PDD(SSD,E,A,d_c) \cdot OAR(SSD,x,y,E,A,d_c) \cdot \frac{(SSD+d_{max})^2}{(SSD+d_{max}+h)^2} \quad (2.14)$$

A situation in which point Q would be under an excess of tissue is treated the same way but with a negative h value. Since the OAR are always measured in 2D (function of depth and off axis position) when doing 3D calculation the OAR(x, y) will be approximated by the product of the two 2D off-axis ratio, (Eq. 2.15). The OAR "factor terms" in Eq. 2.14 include the effect of beam modifiers such as wedges.

$$OAR(SSD,x,y,E,A,d_c) = OAR(SSD,x,E,A_x,d_c)\cdot OAR(SSD,y,E,A_y,d_c) \qquad (2.15)$$

A more sophisticated approximation of the 3D off-axis ratio consist in separating the 2D OAR's in 2 factors, a boundary factor and a radial factor [CHU1]. The radial factor will include such effects as the "horns" and spectral variation of photon fluence across the field. The boundary factor is approximated by the 2D OAR of a broad parallel beam with uniform energy spectrum and fluence across the beam. The 3D OAR is finally obtained by the product of the boundary factors for length x and width y, and the radial factor.

The measured parameters are habitually measured for square fields. When calculating dose for a rectangular field ($A_x \times A_y$), an approximation of the equivalent square field of side A_{eq} has to be found through Equation 2.16 [STER].

$$A_{eq} = \frac{2\cdot A_x \cdot A_y}{\left(A_x + A_y\right)} \qquad (2.16)$$

This approximation works very well for fields of moderate elongation but should be used with care if either A_x or A_y exceeds 20 cm or if their ratio exceeds 2 [DAYA].

Tissue-Air Ratio method

This method is essentially equivalent to the effective SSD method but uses a correction factor C, with a SAD set up

$$C = \frac{TAR(d_c, A_d)}{TAR(d, A_d)} \qquad (2.17)$$

where A_d is the projected equivalent field size at depth d+h. The final corrected dose is found by multiplying this correction factor with the OAR and the dose at depth d_{max} as in Equation 2.14 however the PDD is taken at depth d (along the central axis) and no square term is present.

2.7.2 Tissue inhomogeneity

This type of correction is habitually split into two sub-groups: correction for beam attenuation and scattering, and changes in secondary electron fluence. The relative contribution of these corrections depends where the dose calculation point is with respect to the heterogeneity. For points much deeper than the heterogeneity, the leading effect is the primary beam attenuation. The scattering correction is important in regions closer to the heterogeneity. Finally, the secondary electron fluence is of importance at the interfaces and within the heterogeneity. For high energy beams there is a loss of electronic equilibrium in the vicinity of low density heterogeneities. For lower energy beams the problem is with high density structures like bone in which there is an increase of secondary electron fluence from photoelectric absorption. The absorbed dose within the heterogeneity can thus greatly differ from that in soft tissue. Since corrections for tissue inhomogeneities were not implemented only a brief description of the different methods is presented.

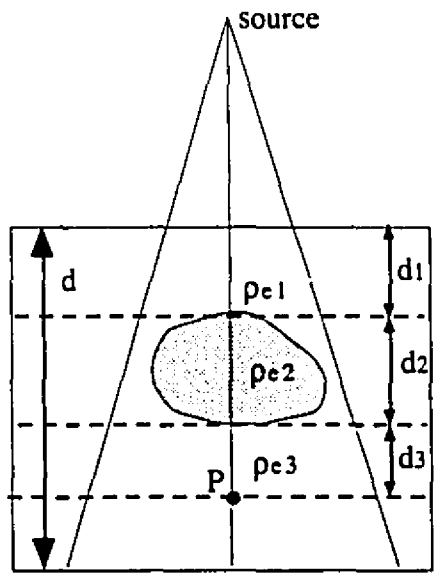

Figure 2.14. Typical heterogeneity approximation.

A tissue-air ratio multiplicative correction factor, Eq. 2.18, similar to the TAR correction factor used for contour irregularities, can be used to correct for inhomogeneitites but the depth d is replace by an effective depth d' which is the equivalent water depth.

$$D_{inh.} = D_{hom.} \cdot C \qquad with \qquad C = \frac{TAR(d', r_a)}{TAR(d, r_a)} \tag{2.18}$$

This is the equivalent radiological path length, i.e. the distance from the position of the calculation point to the entry point of the ray on the patient is scaled according to the equivalent density of water. This is usually achieved either by following the ray in each voxel and scaling the distance traveled within that voxel according to the equivalent electron density that corresponds to the "color" of that voxel (this is obtained through a calibration curve of electron density vs. CT number). This method does not account for the relative position of Q with respect to a certain heterogeneity (the correction factor stays the same as long as d and d' are unchanged). If heterogeneity regions are segmented (as shown in Fig. 2.14), the ray will cross three regions such that the scaled density is given by Eq. 2.19 .

$$d' = \rho_{e1} \cdot d_1 + \rho_{e2} \cdot d_2 + \rho_{e3} \cdot d_3 \tag{2.19}$$

A Power Law Tissue-Air Ratio method proposes a correction factor which is a function of the TAR ratios but now the correction factor does change with a change of d_3, position of the heterogeneity with respect of the calculation point (Eq. 2.20). This method was first proposed by Batho and later extended by Cunningham [CUN0] . The model assumes only Compton interactions and does not apply at the boundaries of the field or in the build-up region.

$$C = \frac{TAR(d_3, r_a)^{\rho_1 - \rho_2}}{TAR(d_2 + d_3, r_a)^{1-\rho_2}} \tag{2.20}$$

Equivalent Tissue-Air Ratio method (ETAR)

This method is again similar to the two preceding ones by its use of a correction factor which is again a ratio of the TAR:

$$C = \frac{TAR(d', r')}{TAR(d, r)}$$
$$r' = r \cdot \tilde{\rho} \tag{2.21}$$

This correction factor actually accounts for the effect of scattering structures and their relative position. This method was proposed by Sontag and Cunningham and not only scales the depth but also the field size where the scaling factor $\tilde{\rho}$ is given by :

$$\tilde{\rho} = \frac{\sum_i \sum_j \sum_k \rho_{ijk} \cdot W_{ijk}}{\sum_i \sum_j \sum_k W_{ijk}} \qquad (2.22)$$

The ρ_{ijk} is the relative density of a scatter element (voxel). The W_{ijk} are the weighting factors assigned to these element in terms of their relative contribution to the scattered dose at the point of calculation. Variations of that method in which the scattered dose is calculated separately or in a single plane are used to simplified the calculation . More advanced techniques use DSR convolution algorithms as explained in Section 2.4 to solve the problem of multiple scatter of photons or electrons specifically at boundaries where electronic equilibrium is not present.

2.8 Dose calculation and corrections in the McGill Treatment Planning System

Since most treatments use an SAD setup a calculation method based on an SAD measured parameter is more appropriate to implement. Therefore a formula for dose calculation that is based on the TMR would be more practical than one based on the PDD as in Eq. 2.14. The beam data in the program are stored as TMR and beam profiles. If the user has PDD data as input measurements they first have to be converted to TMR.

Conversion from PDD to TMR

Starting from measurement data, (PDD and off-axis ratios as explained in next chapter) the program has to calculate the dose to any point inside the volume of the patient with respect to the dose at a normalization point. For an SSD setup, this point is at depth d_{max} under the surface so at SSD + d_{max} from the source. For an SAD setup, this point is at SAD from the source (the isocentre point).

The relation between PDD and TMR is given by Eq. 2.23 and 2.24.

$$TMR(d, r_d) = \left(\frac{PDD(d, r, SSD')}{100}\right)\left(\frac{SSD' + d}{SSD' + d_{max}}\right)^2\left(\frac{PSF(r_{dmax})}{PSF(r_d)}\right) \qquad (2.23)$$

$$\text{where } \left(\frac{PSF(r_{dmax})}{PSF(r_d)}\right) \cong 1 \qquad \text{and} \qquad r = r_d \cdot \left(\frac{SSD'}{SSD' + d}\right) = r_d \cdot \left(\frac{SAD - d}{SAD}\right) \quad (2.24)$$

The geometry is shown in Fig. 2.15.

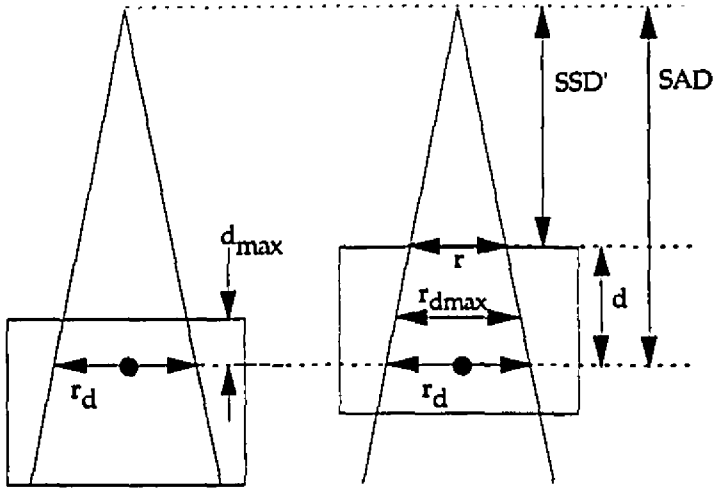

Figure 2.15. Geometry for PDD to TMR conversion.

However, the measured PDD are taken at SSD = SAD of the treatment machine so one need to obtain different PDD, at the modified SSD (or SSD'). This is obtained with the help of the Mayneord Factor [KHAN] Eq. 2.25.

$$PDD(d, r, f_2) = PDD(d, r, f_1)\left(\frac{f_2 + d_{max}}{f_1 + d_{max}}\right)^2 \left(\frac{f_1 + d}{f_2 + d}\right)^2 \quad (2.25)$$

then the PDD measured at SSD=SAD can be corrected to get the PDD at SSD' = SAD-d so that f_2=SAD-d and f_1=SSD=SAD of the specific machine.

Then Eq. 2.23 becomes,

$$TMR(d, r_d) = \left(\frac{PDD(d, r, SAD)}{100}\right) \cdot \left(\frac{SAD - d + d_{max}}{SAD + d_{max}}\right)^2 \cdot \left(\frac{SAD + d}{SAD - d + d}\right)^2 \cdot \left(\frac{SAD - d + d}{SAD - d + d_{max}}\right)^2 \cdot \left(\frac{PSF(r_{dmax})}{PSF(r_d)}\right) \quad (2.26)$$

which reduces to:

$$TMR(d,r_d)=\left(\frac{PDD(d,r,SAD)}{100}\right)\left(\frac{SAD+d}{SAD+d_{max}}\right)^2\left(\frac{PSF(r_{dmax})}{PSF(r_d)}\right) \quad (2.27)$$

Dose Calculation Principle

Starting from the TMR values for an isocentric set-up, the dose at any point (Q) has to be found and normalized to the dose at the isocentre (iso). Therefore, from the geometry of Fig. 2.16:

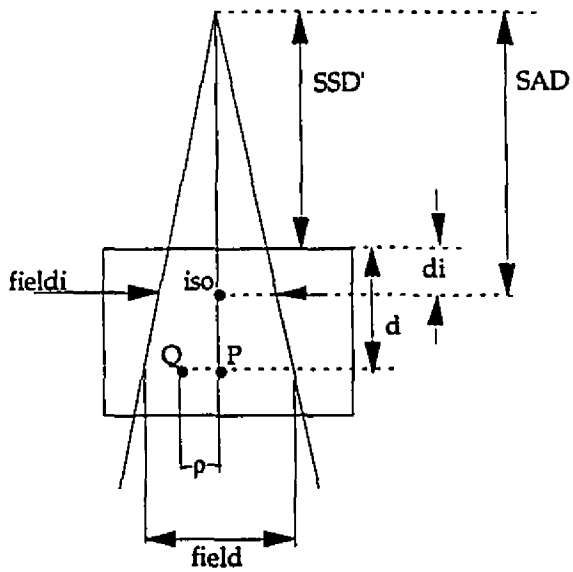

Figure 2.16 Geometry for dose calculation

and from the definition of TMR:

$$D_p=(D_p)_{max}TMR(field,d) \quad (2.28)$$

and from the definition of PSF(F):

$$(D_p)_{max}=\left(D_p\right)' PSF(field) \quad (2.29)$$

and:

$$(D_{iso})_{max} = (D_{iso})' \, PSF(fieldi) \tag{2.30}$$

and since the two dose values in air are related by the inverse square law :

$$(D_p)' = (D_{iso})' \left(\frac{SAD}{SAD + d - di} \right)^2 \tag{2.31}$$

then:

$$\begin{aligned} (D_p)_{max} &= (D_{iso})' \left(\frac{SAD}{SAD + d - di} \right)^2 PSF(field) \\ &= (D_{iso})_{max} \left(\frac{SAD}{SAD + d - di} \right)^2 \frac{PSF(field)}{PSF(fieldi)} \end{aligned} \tag{2.32}$$

thus the normalized dose Eq. 2.33 at point Q is found from 2.28 and 2.32:

$$\begin{aligned} \frac{D_Q}{(D_{iso})_{max}} &= \frac{(D_p)_{max}}{(D_{iso})_{max}} TMR(field,d) \cdot OAR(d,\rho) \\ &= TMR(field,d) \cdot \left(\frac{SAD}{SAD + d - di} \right)^2 \frac{PSF(field)}{PSF(fieldi)} OAR(d,\rho) \end{aligned} \tag{2.33}$$

Eq. 2.34 is the equivalent equation with the PDD value.

$$\begin{aligned} \frac{D_Q}{(D_{iso})_{max}} = PDD\left(d, \left(\frac{field \cdot (SAD - d)}{SAD} \right), SAD \right) \left(\frac{SAD + d}{SAD + d_{max}} \right)^2 \\ \times \left(\frac{SAD}{SAD + d - di} \right)^2 OAR(d,\rho) \end{aligned} \tag{2.34}$$

The PSF ratios are neglected since they are approximately equal to 1. The SAD value of Figures 2.15 and 2.16 are the same, since SAD is a fixed distance for a given treatment machine.

As pointed out by [PCW2] the use of the radiological path length corrects approximately for the surface curvature and the internal structure. Other approaches, such as the ones

described in the previous section, use multiplicative correction factors that require additional computations. The difference between the results of the various methods is not very significant.

Finally, in Eq. 2.33, the OAR is a three dimensional function as found through Eq. 2.15. However since the measurements of OAR are taken with an SSD setup a correction has to be applied to correct for the difference of divergence if one calculates the dose for a SAD setup.

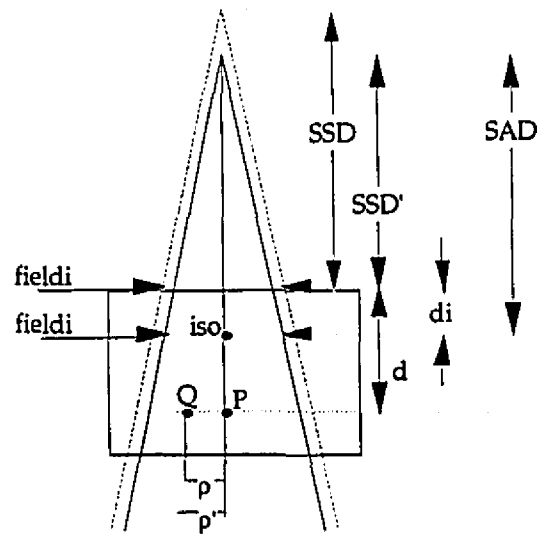

Figure 2.17. OAR correction for divergence.

$$\rho' = \rho \cdot \left(\frac{SSD + d}{SSD - d_i + d} \right) \tag{2.35}$$

Therefore the lookup values of OAR will be for the field size at the isocentre which is "brought" to the surface, at depth along the central axis for the point of calculation Q but the off-axis distance ρ is modified by a geometric factor, (Eq. 2.35).

Chapter 3

Materials and Methods for the Implementation

3.1 Introduction

This chapter presents a brief overview of the capabilities of the McGill Treatment Planning System in order to define more precisely the work required to implement external photon beam treatment planning. The implementation procedure is described next along with some specific data structures and pseudo-codes. The detail given on these structures and code is limited to cover the original goal of this thesis. General description of some existent parts and functions of the program are also given when required. The programming, in C language, and compilation of the program was performed on various Macintosh computers (Apple Computer Inc., Cupertino CA) with the integrated development environment (IDE) CodeWarrior C/C++™ from MetroWerks Inc.

3.2 Overview of The McGill Planning System (MPS)

The McGill Treatment Planning System is a Macintosh based treatment planning system initially conceived for brachytherapy and stereotactic radiosurgery treatment planning. It was developed at McGill University by Dr. Conrado Pla [PLA1]. The program makes use of the Apple Macintosh user interface. All operations are mouse driven except when numeric inputs are required. The program is available for the two Macintosh platforms: the standard CISC based Macintosh computer (68K Motorola processor series) and the new RISC based processors (PowerPC 600's) series which are considerably more powerful when doing extensive computations. Figure 3.1 shows the main options of the program.

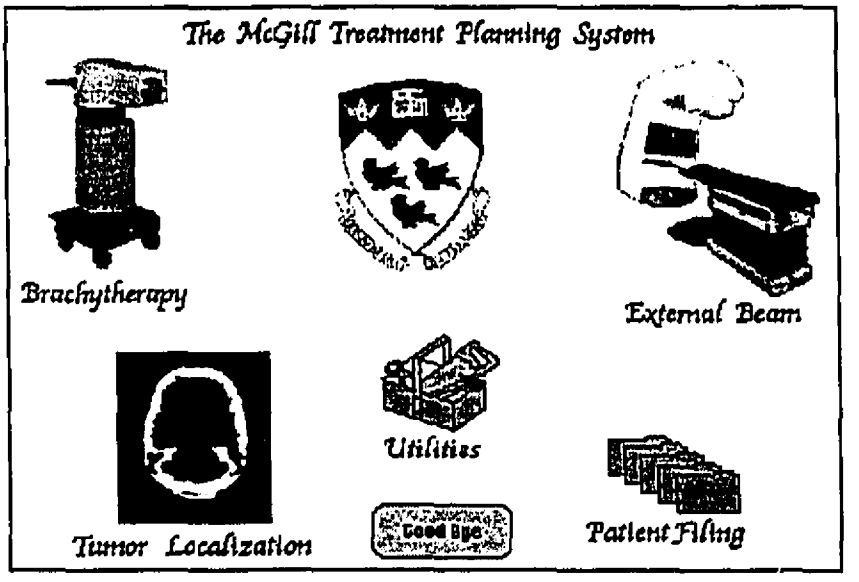

Figure 3.1. Main menu of the McGill Treatment Planning System Program.

The brachytherapy planning allows the user to import a pair of orthogonal films taken with magnification marks that allows precise reconstruction of catheter positions. The radioactive sources are shown with the catheters superimposed on the films for visualization of the loading volume. The dose distribution can then be calculated and viewed in any arbitrary plane. Calculation of dose distribution in sets of parallel planes at arbitrary orientation can be projected on the orthogonal films to visualize the isosurfaces shape.

Stereotactic planning first involves importing the CT or MRI images through video grabbing or through a network. The fiducial markers imbedded in the stereotactic frame which are located on every image allow precise determination of the coordinates of any point in the patient volume. A contour editor is used to create and edit the shapes of various contours: patient surface, tumors and other structures of interest. The next step is to define a treatment isocentre by clicking with the mouse. Several windows are available to help the user with the different operations: (cf. Figures in section 4.1). a "transverse image window" shows the currently selected image; the "Image Index window" shows all available images for the given patient; the "cursor window" shows the coordinates and the dose at the point where the user clicks with the mouse on the transverse or index image window. An "isodose window" is available when the isocentre of treatment is selected and the dose can be calculated; it is used to select the isodose values that are

shown on the transverse image window. Some other useful windows are also available: a "stack view window" which may also include a sagittal and coronal reconstruction, a "dose volume histograms (DVH) window" of the tumor and the surrounding tissue, a "beam eye's view window", a "beam information window" where the user is shown the characteristics of each beam, etc..

When the user selects an isocentre with the mouse cursor, the program brings up a "dialog window" in which the user chooses a particular stereotactic treatment technique, treatment machine and a field size for the selected treatment machine. Once these selections are made it is possible to calculate the dose at any point inside the patient volume. The dose distribution can be visualized in each image plane, Fig. 4.3. It is also shown (in the stack view window) in transverse, coronal and sagittal planes, Fig. 4.4. It is easy for the user to try out different planning set-ups, such as changing the beam sizes, beam angles, the number of beams and location of the isocentre.

3.3 General approach for implementation

The general approach for implementation of the external beam routines has to consider the current arrangement and manipulation formalism for the data in the program. Most of the existing data structures and functions designed for brachytherapy and stereotactic planning are also applicable to external photon beam planning. In particular, the interface for the stereotactic treatment planning, described above, is well suited for doing external beam treatment planning. The manipulation of CT images and of external beam machine data is required in both cases. The main difference between external photon beam planning and stereotactic treatment planning is the number of treatment beams, their sizes and the size of the target volume. Therefore the principal work to adapt the McGill treatment planning system to do external beam treatment planning involves generalizing the dose calculation algorithms to handle large treatment beams. Not only the dose calculation algorithm has to be generalized but also the way beam data is generated, the method by which the dose is stored and the method by which patient data is localized in space.

The existing dose calculation algorithms for stereotactic beams were simplified by using adequate approximations to speed up the calculations: the surface of the patient was assumed to be flat and therefore the depth of each calculated points within the volume

was well determined from the depth of one point, the treatment isocentre, located on the central axis of the beam. When doing 3-D external photon beam treatment planning such assumptions do not hold. The calculation of dose in 3-D (based on measured data) requires the knowledge of the depth of every calculation point, as explained in Section 2.7. As pointed out by many researchers, [STAR], [SID1], the critical step in the dose calculation process is the depth searches, or equivalently the problem of finding the entry point on the patient volume for every calculation point. This operation can take up as much as 85% of the dose calculation time for a 3-D system. For this reason some effort was put into accelerating the 3-D depth searches for our system. A depth search based on the use of polar coordinates for contour points and triangular surface patching of the patient skin is the solution which has been chosen to implement and this will be described in Section 3.7. Moreover this surface patching can be used to show a 3-D surface rendering of the patient volume. When doing 3-D treatment planning it is very important to have some tools for visualizing the treatment set-up and the patient geometry. This is why some work was also done to implement a user friendly interface for manipulating and visualizing the patient data, through an Observer Eye's View (OEV), and the treatment setup (couch-gantry) in a 3-D rendered perspective projection.

3.4 Data Structures Organization

The efficiency of a computer program written in C code depends heavily on the organization of the data structures. A *structure* in C is defined as a group of related variables that is given a specific name and will act as a specific variable. It is possible to create an array of a specific data structure. It is usually more efficient to directly define the array in memory with the use of pointers (that point to specific positions in memory) since the size of the array can be modified to contain exactly the number of desired elements. Nowadays, most computers including Macintosh, use dynamic memory allocation to maximize the size of continuous allocable blocks (free memory). For these machines, the concept of pointers is not sufficient anymore since when a block of memory is re-sized, it may be rewritten in a different memory location and the previous pointer would then become invalid (not pointing to the new location of data in memory). To overcome this problem the Macintosh computers use handles, or "pointers to pointers": a handle defined with a specific byte size will be moved in memory as a whole block. This block may also be locked temporarely to stay fixed in memory when accessing elements of the handle with another pointer, for example in a loop that reads or

writes all elements of the handle. In the following discussion, pointers are preceded by a "*" sign (e.g.: *Pointer_Name). Handles, that is "pointers on pointers", are preceded by "**" (e.g.: **Handle_Name). A handle could be seen as a relocatable array of a given structure or variable.

Well designed data structures are an easy and efficient way to "pass" and "return" relevant data information between functions. Expanding a program is also much easier when the design of the structures is planned for future development. The MPS program has always followed this philosophy and for this reason many existing data structures were used "as is" for the present implementation. The important data structures that are used for external photon beam treatment planning can be categorized in two groups: structures representing patient data and structures for treatment data.

3.5 Patient Data Structures

The patient data structures are those containing the information on the patient anatomy. One handle of the structure TLIndexRec has one element for each slice. It contains most of the patient information. This structure was originally defined for stereotactic treatment planning but it is also very adequate for containing patient information for external beam treatment planning. This structure contains a handle of the slice images, and various important information such as the thickness of the slice, bezier representation of the various structure contours in that particular slice, a list of points in image coordinates sampling the patient contour, the plane equation (cosine director of the normal of the plane in frame coordinates) of that slice, the type of reference frame, etc. The patient information is also saved on disk in particular file formats: a series of image files ("packed images") one for each slice image of the patient, and one image index file that contains the other information and characteristics of the images.

A very important concept is the different coordinate systems in which the patient data can be manipulated. Each of them are used in particular situations where they simplify the manipulation of the data. For example, when finding quantities that are relative to the isocentre of treatment, the isocentre coordinate system is more adequate to represent the location in the patient volume. The *McGill Treatment Planning System* uses 4 different types of coordinate systems: the *image coordinate system*, the *isocentre (or couch)* coordinate system, the *frame* coordinate system, and finally the *polar* coordinate system.

The latter was implemented especially for external beam treatment planning. The various coordinate systems are illustrated in Fig. 3.2.

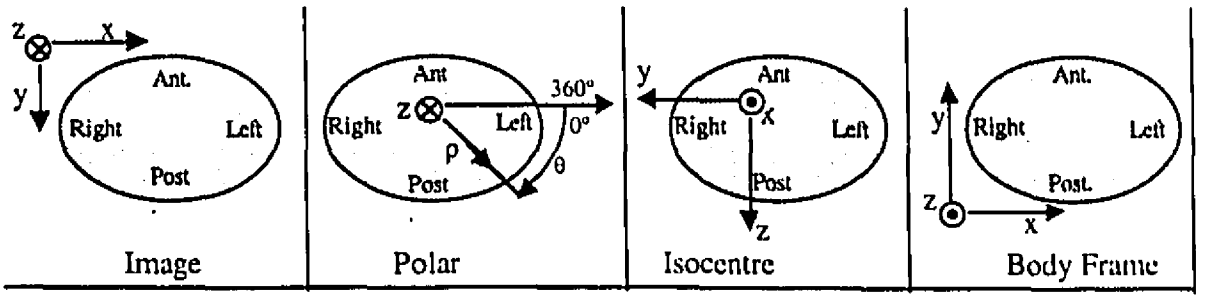

Figure 3.2. The various coordinate systems. The direction of the third dimension (axis going in or out the plane) is indicated by a cross hair (pointing in) or by a dot (pointing out).

The image coordinate system is really a 2-D coordinate system equivalent to the screen coordinate system of the image in the window where it is displayed, the origin being at the top left corner of the image. The image coordinate system is needed to link the display of the image slices in window coordinates to the other coordinate system for example when the user clicks on an image, this position has to be defined also in the other 3-D coordinate systems. The polar coordinate system is directly based on the image coordinate system but the origin is at a different location. The isocentre (or couch) coordinate system has the 3-D location of the isocentre of a treatment for origin. The x-axis is about the direction of the couch and the z and y-axes are equivalent respectively to the -y and -x-axes of the frame coordinate system, (Fig. 3.2). This frame is useful when dealing with coordinates relative to the isocentre of treatment. Finally, the frame coordinate system is probably the most important since it is the one that makes possible the precise 3-D localization of any point in space. For stereotactic treatment images, fiducials markers from the particular localization frame that is used allow precise construction of the 3-D image plane equation in the coordinate system of the frame. The position of the reference point (0, 0, 0) and orientation of the orthogonal set of axis depends on the frame type. Since there is no physical frame in external beam planning, a virtual "body" frame coordinate system based on the scanner images information was implemented in order to extend the use of existing routines which assume the existence of a frame. The body frame is based on the geometry of a Leksell Frame with the origin point moved further away so as not to be situated inside the patient volume (Fig. 3.3).

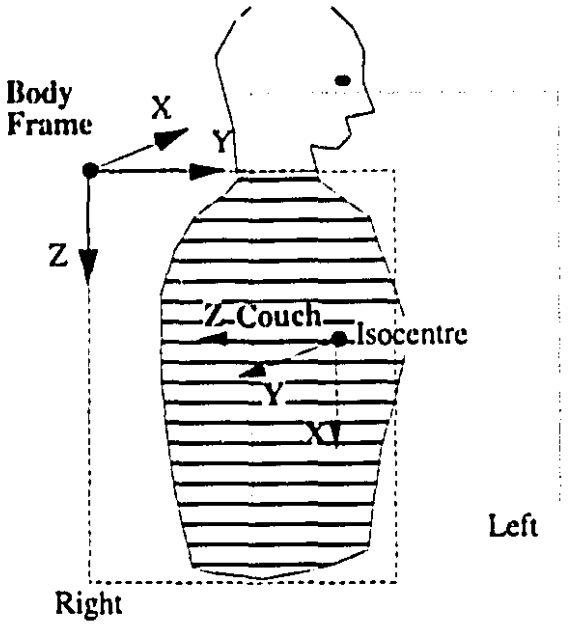

Figure 3.3. The virtual "Body Frame".

The polar representation of the patient contour was required for faster localization of entry points, to simplify the surface representations and to facilitate 3-D rendered display of the patient volume. The polar segmentation routines and data structures were designed to be general enough so they could be used for other applications such as polar segmentation of an irregular field before performing a Clarkson integration [CLAR].

3.5.1 Polar Represenation

This polar representation will be applied to the contour points of each image slice. To produced a polar representation that can be applied to any situation some special considerations are required. First of all, a valid polar representation should be obtained regardless of the location of the polar origin (located inside or outside the given contour) and on how tortuous that contour is. The polar representation is therefore not assumed beforehand to be single-valued. The data structure for the polar information is illustrated in Fig. 3.4 . A polar contour handle is used to represent the whole set of external patient contours, each element of the handle being one slice contour of the patient represented by the PolarContRec structure. The "step" element indicates the angular sampling step, "max" and "min" are respectively the maximum and minimum angle sampled for that slice, "npoint" is the number of samples for that slice, "jumpup" and "jumpdown" are used to indicate a jump in the angular sampling, i.e. an angular span where there is no sample. "PolarIso" is the coordinate in image coordinates of the polar origin. The two last elements are handles. The sampled polar points are contained in the **PolarRaster

handle, which has "npoint" elements PolarPoint, of increasing sampling angle and radius, that contains three elements: the angle and radius of that point and a boolean flag indicating if the next point of the list is also sampled at the same angle. "StartRaster" points to a list that contains long integers values, each pointing on the element of **PolarRaster where a given sampling angle starts. For example, if "step" is 10° and "min" is 0°, if there is 3 sampling values at 0° the first element of StartRaster is 0 and the second elements is 3. This classification allows all possible sampling situations. Figure 3.5 gives an example of a sampling contour.

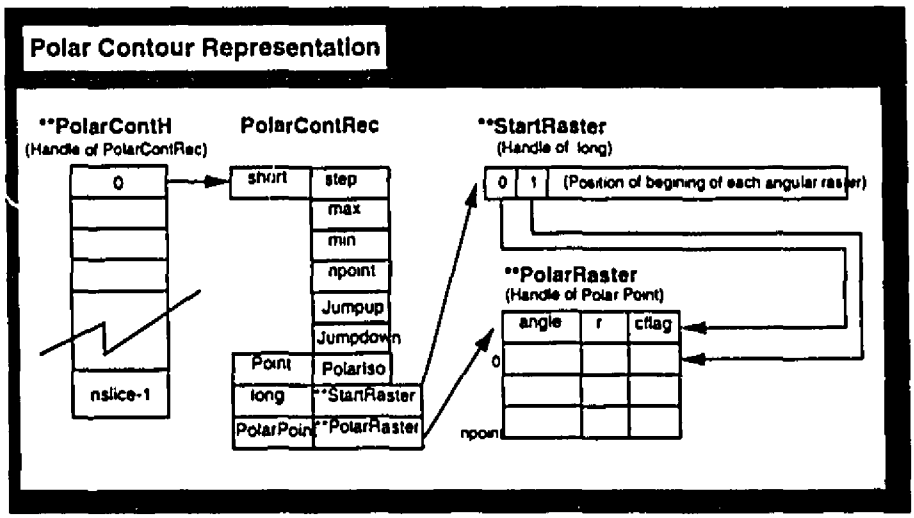

Figure 3.4. The Polar Contour Record structure.

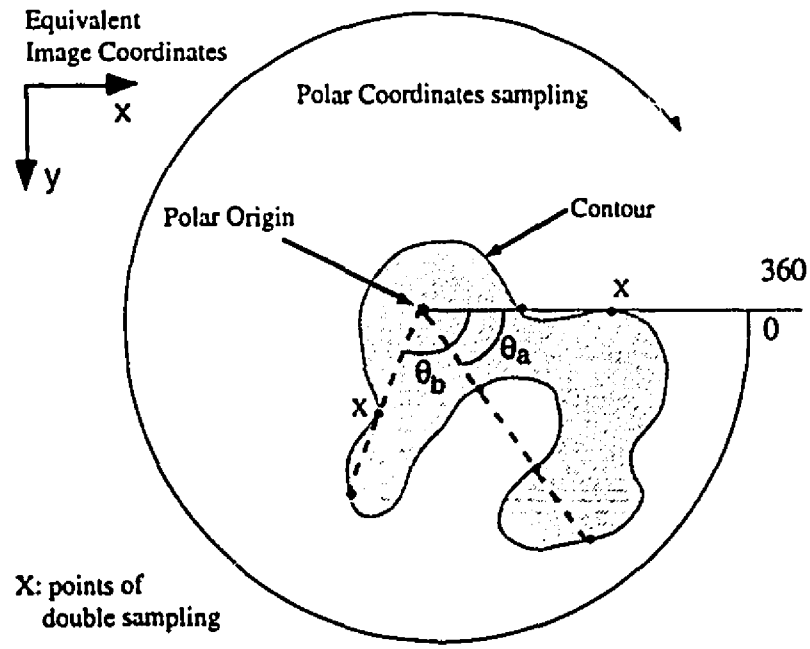

Figure 3.5. Example of a polar representation of a winding contour.

In the example shown in Fig. 3.5, two interpolation angles are illustrated at θ_a and θ_b : for θ_a, there are three points (of different radii) and for θ_b, there is also 3 points since X is at a position where the angular direction changes, therefore it is sampled twice. This makes localization easier since starting from the polar origin, for instance positioned inside the contour, a given raster is easy to follow. The first point of that raster indicates that the raster (line from the polar origin towards the exterior at the given polar angle) is going out of the contour. The next point means that the raster is coming back inside, etc.

The method for keeping track of the jump that occurs when the PolarOrigin point is outside the contour is illustrated in Fig. 3.6, where the origin is placed on the left side of the contour. In that case the min and max angle will still be 0 and 360. However there are two important angles to consider for finding the angular region spanned by the contour. These two angles are "jumpup" and "jumpdown" in the PolarContRec.

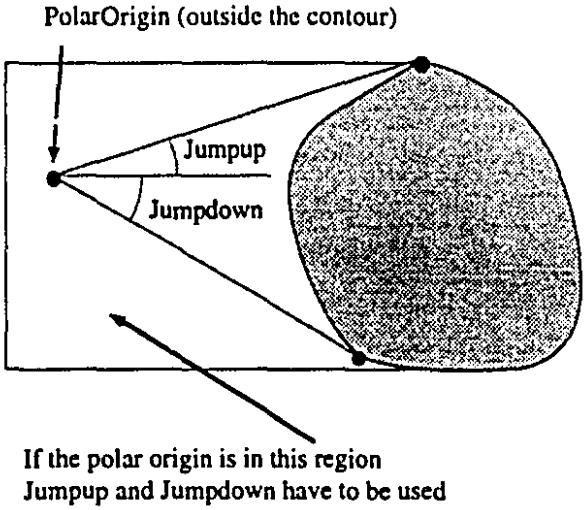

Figure 3.6. Polar origin outside of contour on the left side.

In cases where the polar origin point is outside of the slice but not on the left side the fields "min" and "max" angle will not be 0 and 360 , and therefore indicate the angular span of the slice directly.

The method used for the polar interpolation is simply an angular interpolation between the sampling contour points available in image coordinate. The points in image

coordinates are first obtained from a sampling on the bezier representation of the contour that is drawn by the user on the image when loading new patient images.

3.5.2 Triangular Patching for Representation of Patient Surface

Most of the patient contours that are encountered when doing external beam planning will be rather regular i.e. "not very winding". Starting from this assumption it is possible to assume that the polar representation will be a single-valued function of the angle i.e. $r=f(\theta)$, and therefore each contour will have the same number of sampled polar points which in turn simplifies the surface representation of the area between two contours of particular image slices. The usual way to create a surface representation of a 3-D volume is by creating 3-D polygons that approximate the surface of the volume. Sophisticated algorithms are known to perform this for any arbitrary contour points [LAUR]. In our case, however, a regular polar interpolation is performed on each of the contours at a specific angle step and it is easy to link the points from one contour to the next with 3-D triangles having vertices at every second sampled point (cf. Fig. 3.7). This type of surface representation is acceptable for sampling angles less than or equal to 10 . For example, a typical patient data set composed of 30 image contours, a 10 polar sampling, will produce 2088 triangles each having 3 vertices and a plane equation.

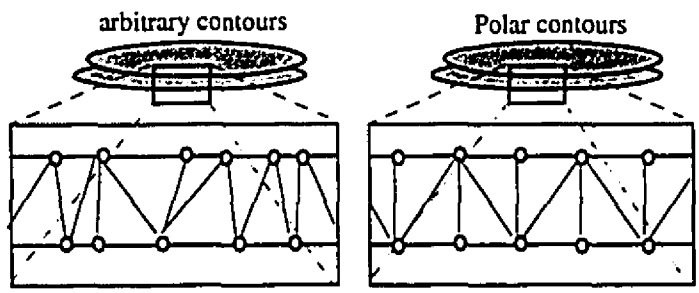

Figure 3.7. General polygon surface patching vs. indexed triangular surface patching.

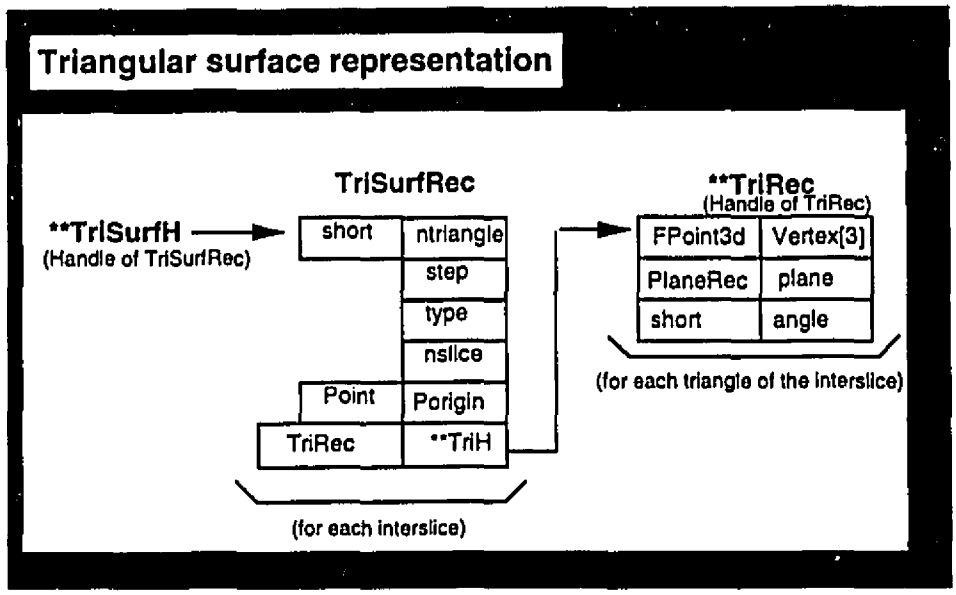

Figure 3.8. Structures for triangular representation.

The patching process requires its own data structures to simplify its implementation. Figure 3.8 illustrates the structure that was used. The **TriSurfH is a list of all the regions between slice ("interslice"). Each element is a "TrisurfRec" structure that contains variables for the number of triangles ("ntriangle"), the interpolation step size ("step"), the type of contour for future use ("type") , the number of interslice regions ("nslice"), the polar origin in image coordinates ("Porigin") and finally a list of triangle elements "**TriH" for the particular interslice. **TriH contains elements of TriRec structure, each one having three 3-D coordinates in frame coordinates: the vertices of a particular triangle ("Vertex[3] array"), the plane equation of that triangle, and the polar angle of that triangle ("angle").

The polar origin point ("Porigin"), which is common to all the slices, defines the origin for the polar interpolation. It is obtained by taking the intersection of all the best fit rectangles of each slice image and then taking the coordinate of the center of this rectangle. Some procedure should be used in the eventuality that the intersection is null, for example shifting the Porigin of one contour until an intersection is found. Another problem that may occur is when the contours are not smooth enough for $f(\theta)$ to be single-valued; in this case one should either smooth the contours, or if the shape really forbids the single value assumption the patching algorithm should be modified to a general triangulation. The general triangulation algorithm is more general but the triangulation based on polar coordinates gives some indexation of the surface position of the triangles

(angular position) which simplifies the depth searches on a plane grid, as will be shown later.

3.6 Treatment Data Structures

3.6.1 Beam Data

The system was tested with the beam data from a Varian Clinac 2300C/D (18 MV beam). The measured data, PDD (or TMR) and OAR values are stored in a text file for various square field sizes from 2×2 cm^2 to 30×30 cm^2. When the program does the calculation for a planning session with a specific treatment machine, it first reads the beam data file of the machine and from it generates other beam data at regular sampling intervals to ensure faster and easier lookup of the required values when doing dose calculations. For external beam planning this procedure has to be different from the stereotactic beam data generation. Basically, the same parameters are generated (TMR and OAR). However, the sampling intervals do not have to be as small as for stereotactic beam data. Stereotactic beam data are typically generated at every 0.25 cm for circular field sizes from 0.5 cm to 4 cm in diameter and for depths from 0 to 30 cm at every 1 mm. For external beam, it is more appropriate to generate field sizes at every 2 cm, from 2 cm to 30 cm for square fields, and for depths ranging from 0 to the maximum available depth at intervals of 1 mm. The OAR data for external beam has to be more elaborated than for stereotactic beams. The divergence of external beam is much greater so the shape of the profiles will change considerably with depth. The profiles of stereotactic beams are assumed to be very similar with depth and therefore they were only interpolated and stored at one depth for each field size. However for external beam they are stored and interpolated at 5 different arbitrary depths; in our case these depths are at d_{max}, $d_{max} + 8$ cm, $d_{max} + 16$ cm, $d_{max} + 24$ cm, $d_{max} + 32$ cm). Therefore for a 18 MV beam, where dmax is 3 cm, the depths are 3.0, 11.0, 19.0, 27.0, and 35.0 cm. The calculated beam data are stored in the same handles (**tmrH and **oarH, cf. Fig. 3.9) for both external beam and stereotactic beam. These handles are simply one dimensional arrays of floating point numbers.

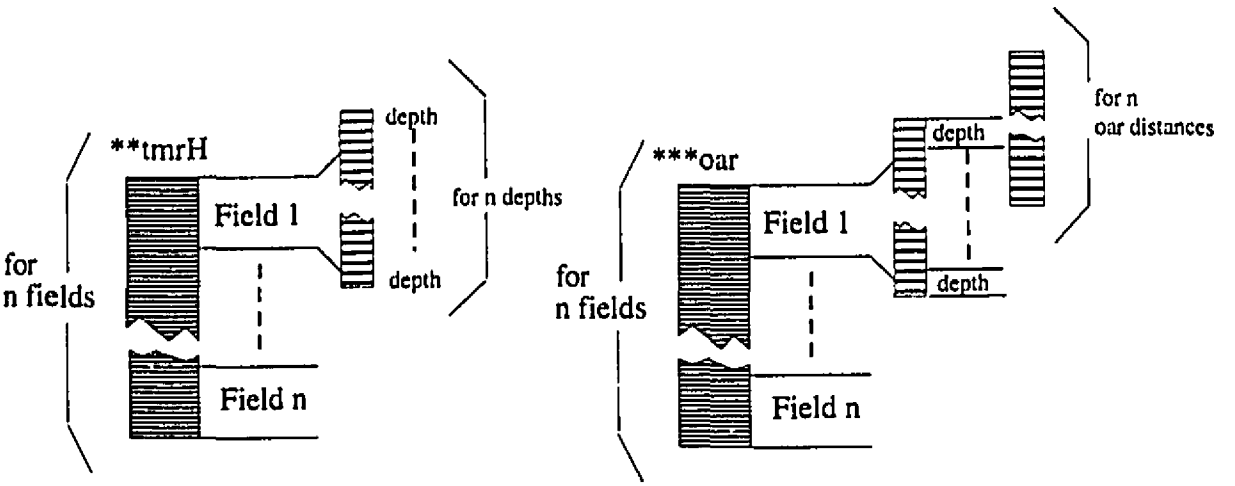

Figure 3.9. Structures for efficient storage of beam data.

If PDD are provided in the beam data file, the required TMR values are calculated using Eq. 2.27.

3.6.2 Calculation grid and dose matrix

The calculation grid used in stereotactic planning, defined on each image slice, is a variable grid reduced to the small area where dose is deposited. For external beam calculations such a a simplification is not appropriate since most of the area of the slice is likely to receive some significant dose. The grid has to be extended to fully cover the slice, as shown in Fig. 3.10, although it does not need to have variable resolution.

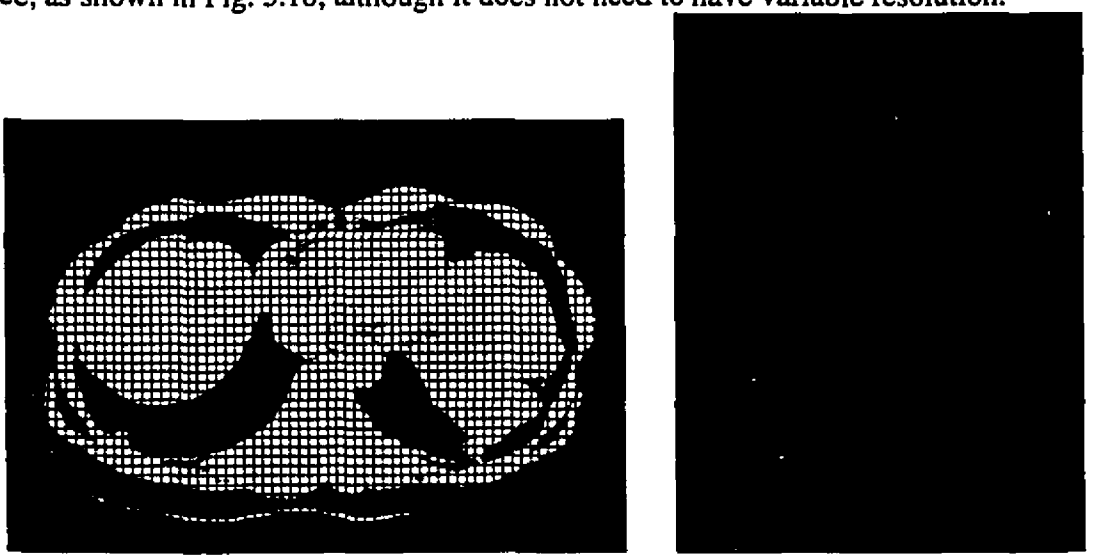

(a) (b)

Figure 3.10. Typical calculation grids. (a): a regular 5 mm square size grid used in external beam treatment planning. (b): irregular grid for stereotactic treatment planning.

In the planning interface, the user has the option to change the calculation grid size (Fig. 4.2). The grid size affects the precision of the calculation since the dose is calculated only at the grid points. The calculation planes are defined in three dimensions, in the plane of the slices. The calculation time is obviously proportional to the number of grid points. The results of the dose calculation for each slice are stored in a dose matrix, which is a one-dimensional array, each element corresponding to the dose of particular grid point.

3.6.3 Treatment specification

The treatment delivery parameters are stored in a particular structure, "StTreatRec". This structure contains the definition of the calculation grid, the number of isocentres for the treatment technique and the particular beam settings and weightings that belongs to each isocentre. The beams that are applied to each isocentre can either be normal fixed beams ("free") or arcs. For calculation purposes, a free beam is an arc that consist of a single beam. For each of these free beams or arcs a set of parameters is stored; this includes the couch, gantry and collimator angle, the beams energy, the type of collimation and its size, the depth of the isocentre for this beam, etc.... This structure is filled in when the user defines the treatment technique with the help of a user dialog (as shown in Chapter 4). Future versions of the program could also integrate a 3-D graphical user interface for definition of the treatment techniques (isocentres and beams characteristics) taking advantages of the capabilities of the interface described in Section 3.9.

3.7 Fast depth calculations

General approach for depth searches

The depth of a point given its 3-D coordinates (x, y, z) in a given coordinate system and its cosine directors has to be found. The cosine directors give the direction of the ray towards the source position. The coordinate system was chosen to be the body frame

coordinate since the dose calculation planes are already in the coordinate of this frame and so are the coordinates of the 3-D contours points of triangles in **TriSurfH.

A straight-forward way of finding the depth of a specific point with respect to the source is to find the two "bracketing" slices in between which the ray crosses the surface. If there is no such pair then the ray must be entering from the top or bottom slice. The bracketing of the two slices is obtained in the following way:

çcheck top and bottom image/ray intersection (through specific routines that verify if the intersection of the ray in the plane of the image is within the boundaries of the image contour).
çthen, depending of the direction of the ray, check from the top or from the bottom for an inside image intersection.
çwhen this intersection is found, the bracketing slices are determined.

Next, the closest point to the ray on each of the two contours is found and from these two points a linear interpolation is performed to find the depth, see the geometry in Fig. 3.12 b.

This method is tedious in the sense that for each calculation of depth two slices have to be bracketed and for each one the closest point has to be found. This method would be used as an alternative to the other one in case the assumption of the smooth varying contour cannot be applied.

Depth searches with Triangular Surface Patching

The main goal of this method is to speed up the depth search. Section 3.5.2 described how a triangular representation of the surface is obtained and arranged. Since the triangles are classified by angle, the search can be indexed. In order to find the depth of a calculation point, a means of finding the intersection of a ray with one triangle structure is required. The algorithm that performs this is illustrated in Fig. 3.11 [GLA0]. The ray is defined by a parametric equation with parameter t: $\vec{r}(t) = \vec{O} + \vec{n} \cdot t$ where $\vec{O}$ is the 3-D coordinate of the origin of the ray (calculation point) and $\vec{n}$ is a unit vector along the ray towards the source. The triangle definition (as previously defined) is composed of three 3-D vertices V_i and a plane equation $\vec{N} \cdot \vec{P} + d = 0$ where $\vec{N}$ is the normal unit vector of

the plane, $\vec{P}$ is an arbitrary point of the plane and d is the shortest distance of the plane from the origin.

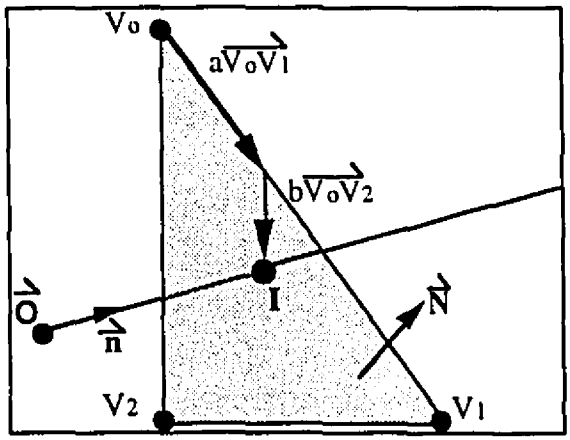

Figure 3.11. Parameters for ray-triangle intersection algorithm.

Equation 3.1 returns the parametric value at which the ray intersects the triangle plane and therefore gives the intersection point $\vec{I}$. Then to verify if this point is located within the boundary of the triangle, the vector from one vertex (V_0) of the triangle to the intersection point (I) is expressed as a linear combination of two vectors (V_0V_1 and V_0V_2) Eq. 3.1 (2). If the conditions of Eq. 3.1 (3) are satisfied, the intersection point is within the triangle.

$$\begin{bmatrix} t_i = -\dfrac{\left(d + \vec{N}\cdot\vec{O}\right)}{\left(\vec{N}\cdot\vec{n}\right)} \\ I = \vec{r}\left(t_i\right) = \vec{O} + \vec{n}\cdot t_i \end{bmatrix} \qquad (1)$$

$$V_0I = a\cdot V_0V_1 + b\cdot V_0V_2 \qquad (2) \qquad (3.1)$$

$$\begin{Bmatrix} a,\ b \geq 0 \\ a+b \leq 1 \end{Bmatrix} \qquad (3)$$

When finding the intersection of a given ray with the whole patient surface, not all triangles will be tested for intersection with this ray, since this would be rather a slow process. The possible entry angles of the ray are limited: the intersection point of the ray with the contours must be between the angle θ spanned by the Polar origin to source angle and the Polar origin to intersection point of the ray within the slice Fig. 3.12 (a). Also the

intersection cannot be lower (dot-product wise) than the point, i.e. the search should be performed from the closest slice of the point toward the top or bottom of the volume (cf. Fig. 3.12 (b)). These two assumptions speed up the search considerably. Moreover, the search is limited to the triangles included in the intersection of the full beam with the patient surface plus a certain boundary (as illustrated in Fig. 3.13) necessary to calculate the depth of points in the penumbra of the field.

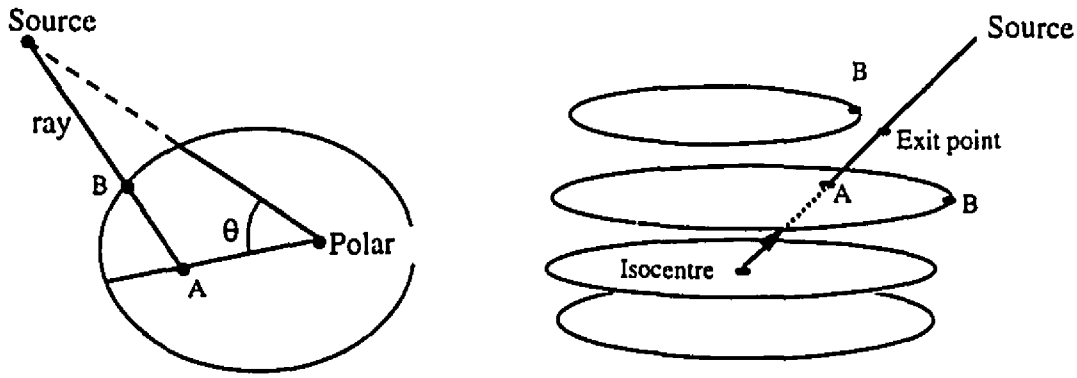

A: Intersection of the ray with the plane of the slice in 3D
B: Intersection of the ray with the slice contour in 2D

(a) (b)

Figure 3.12. The angle range for the entry points (a) and bracketing slices (b).

An additional increase in speed can be obtained by noting that when the depths are calculated to find the dose on the calculation plane by scanning the grid point by point, the depth of one point with respect to an adjacent point will not only be very close but the intersection points on the surface will also be very close to each other, (cf. Fig. 3.13). The depths of each calculation point on the calculation grid is found one by one by rasterising the grid as shown in Fig. 3.15. From one depth search to the other, the position of the previous triangle where an intersection was found is kept in memory. The depth search algorithm will look for successful intersection of the ray with this previous triangle and other adjacent triangles on the patient surface until a successful intersection is found. In general, this method will yield fast depth searches since only a few triangle-ray intersection checks have to be performed.

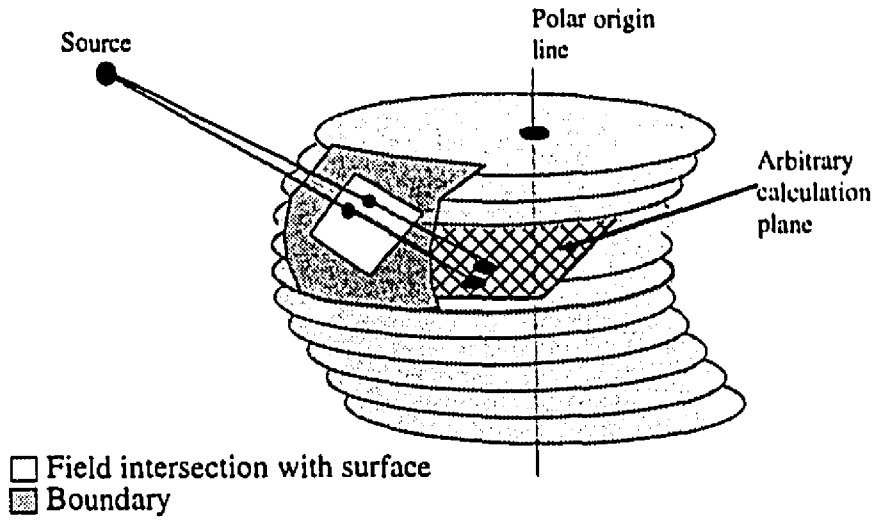

Figure 3.13. Geometry for the depth search.

The time required to find the depth of all grid points is drastically decreased with this method (by about ten times). The angle at which the beam enters the volume with respect to the polar origin will also affect the search's time. The grid should be scanned in a direction parallel to the central axis of the beam to increase the speed, (cf. Fig. 3.14). Since the dose value at the points of the grid that are far enough from the central axis is essentially zero, the dose calculation algorithm can skip the calculation of the dose at these points.

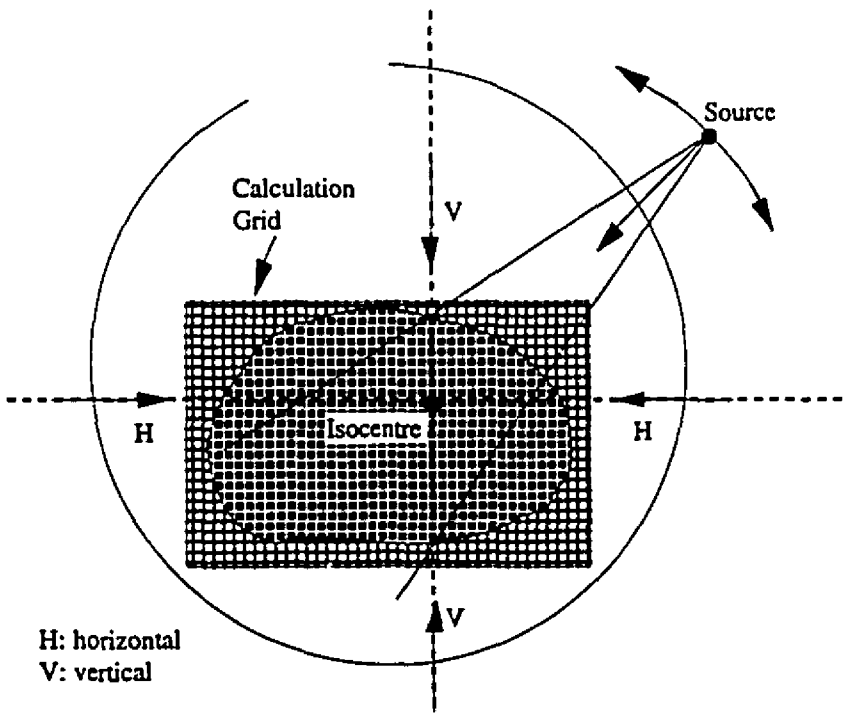

Figure 3.14. Optimization for grid scanning.

The more parallel these points are from a raster (cf. Fig. 3.15), the faster will be the dose calculation since more continuous calculation points can be skip along the rasters. The direction of the grid scanning can either be horizontal or vertical. The angle between the source and the treatment isocentre will determine if the scan will be horizontal or vertical depending whether the unit vector, pointing from the isocentre to the source, has a greater component in the horizontal or in the vertical direction. The raster scan is also "wrapped" i.e. it is as shown as in Fig. 3.15 with P0 being the initial point. This assures that each calculation point is spatially close to the previous one to speed up the algorithm.

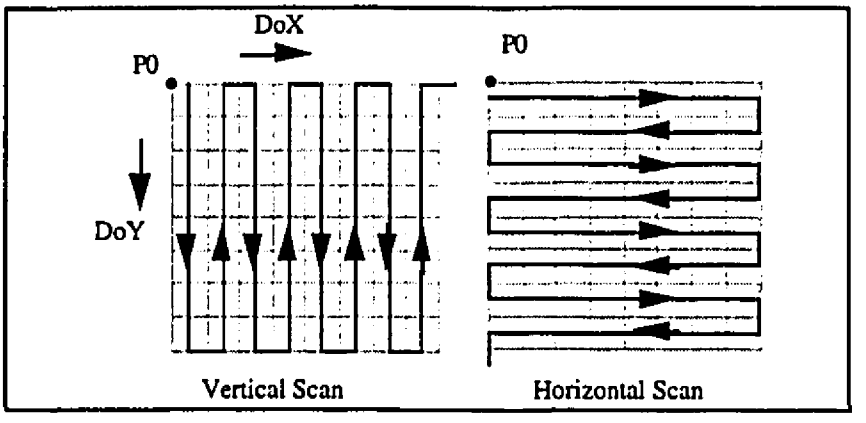

Figure 3.15. Exploring the calculation grid by wrapping the rasters.

3.8 Dose calculation algorithms

The calculation of the dose in a 3-D geometry can be performed when the depth of each calculation point is known. To simplify the implementation, our treatment planning system neglects the effect of tissue heterogeneities. Therefore, only the surface of the patient is considered in finding the geometrical depth of the calculation points, no further density scaling is performed for rays crossing heterogeneities. The inhomogeneity corrections could be applied in future versions by finding the intersections of the ray with the different approximated surfaces of the volume, each surface defining the boundary of a volume of a specific density. The final radiological depth would be approximated by scaling according with the density (as in Eq. 2.19). Each tissue structure that has an approximately constant specific density could be contoured (e.g. lungs, bones, etc.) the same way as before: a polar contour would be found and the triangular surface approximation found for each of these structures. For simplification, the current implementation is only for rectangular fields, leaving irregular fields to a future version. Wedged fields can be used as long as their respective TMR and OAR values are provided

in the beam data file, the dose calculation procedure being the same since the effect of the wedge is taken into account by the beam data.

When a specific treatment technique has been defined by the user, it is possible to calculate the dose in the image slice where a calculation grid is defined by default. In practice the dose calculation can take place in any arbitrary plane where a calculation grid is defined. For every isocentre, for every arc, for every beam, for every point on the calculation grid, the dose is calculated with Eq. 2.33 according to the order of Fig. 3.16. Also, not mentioned in this figure, the TMR value at the calculated point is bi-linearly interpolated from the TMR tables. The OAR value is also interpolated from the OAR tables and the off-axis distance and then scaled accordingly for divergence correction as in Eq. 2.35. The correction for divergence of the beam was verified by comparing the calculations with measurements, (cf. Chapter 4).

```
initialize the dose matrix array to 0 at every grid position.
        for (every isocentre)
                for (every arc)
                        for (every beam)
                                For every grid position (as above wrap around raster)
                                        find depth of the point  (from above techniques)
                                        dose = dose from (Eq.(2.33)) for this beam
                                        dose at this grid point = dose at this grid point+ dose
                                next (grid position)
                        next (beam)
                next (arc)
        next (isocentre)
```

Figure 3.16. Pseudo-code algorithm for dose calculation in a grid plane.

The calculation procedure shown in Fig. 3.16, is used when the user first defines a treatment technique. If some changes are applied to this technique, the program does not necessarily go through the same procedure to update the dose. If some beams of the initial technique have not changed they would not necessarily have to be recalculated. If the number of modified beams times two, plus the number of removed beams and the number of new beams of this new modified technique is less than the total number of beams of the previous techniques, an alternative algorithm is applied (Fig. 3.17).

```
if (modification addition or deletion of isocentre, arcs or free beam(s))
{----------------
 if (((# of modified)*2 + # of removed + # of added) < (total # of beams of previous technique))
  { for (every removed beam)
        For (every grid position) (as above wrap around raster)
              find depth at that point (for removed beam)
              find the dose with from old beam = dose
              dose at grid position = dose at grid position - dose from old beam (from Eq.2.33)
        next (grid position)
   next (removed beam)

 if (modified beam or new beam)
 {       for (all modified or new beam)
              for (every grid position)
                    find depth at that point (for old and new beam)
                    find the dose from old and new beam (from Eq. 2.33)
                          dose at grid point = dose at grid point - dose from old beam
                                                + dose from new beam
              next (grid position)
        next (new or modified beam)
  }
}----------------
else (do like in Fig. 3.16)
```

Figure 3.17. Pseudo-code algorithm for dose calculation in a grid plane.

The algorithm could in the future be improved by incorporating heterogeneity corrections factors, as described in Chapter 2. The only modification required to the algorithm is then to change the depth value at the point of calculation by changing the depth search procedure, taking into account substructures of various densities, previously contoured.

In order to verify the dose calculation algorithm, a "virtual" box phantom was created, (cf. Fig. 3.18). The program already has a function that creates a spherical phantom to perform quality assurance measurements for stereotactic treatment planning. These virtual phantoms are created by generating a set of images or contours defining axial cuts of the phantom. Then the "packed" images and the image index are saved on disk. It is possible to perform all the treatment planning operations of the program on the virtual water box phantom. Since calculation of dose from measurements in a real water tank phantom is a standard procedure, it is then easy to compare the dose calculation results from the program with measured values.

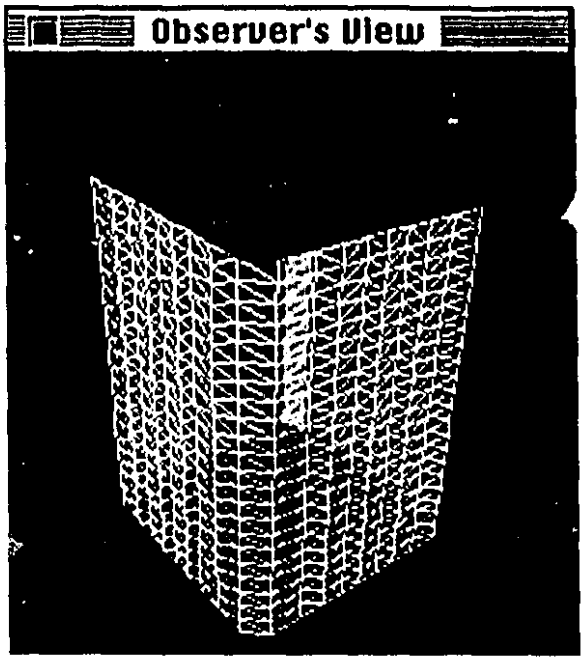

Figure 3.18. OEV of the "virtual box" water phantom, with wire-frame surface and rendered back surface.

3.9 Visualization Tools with the virtual sphere algorithm

A user interface that simplifies the task of visualizing the 3-D information available for the treatment planning was implemented. The virtual sphere algorithm chosen makes possible real time rotation of a 3-D object. The rotated object is viewed through a perspective projection. The algorithm is used in both the BEV and the display of the treatment set-up.

The implementation of the virtual sphere algorithm was based on an algorithm described in [CHEN]. A 3-D virtual trackball is used to rotate an object in space. The user clicks with the mouse within a circle which represents a 2-D projection of a hemisphere (Fig. 3.19). The object (or the set of objects) will rotate with respect to their position relative to the centre of the sphere. The position of the first mouse click (1) defines a point on the sphere (the radius vector α); the next position where the user moves the mouse (2) defines a second position (radius vector β). The cross product of the two vectors produces the vector γ around which the rotation is to take place. The rotation angle θ is the angle spanned by the two initial vectors with respect to the center of rotation. Then the rotation

of the object is calculated and the display updated. Then as the mouse is moved, point (2) becomes point (1) and a new point (2) is updated to the new mouse position. If the computer is fast enough the user has the impression of virtually grabbing the object in space and rotating it.

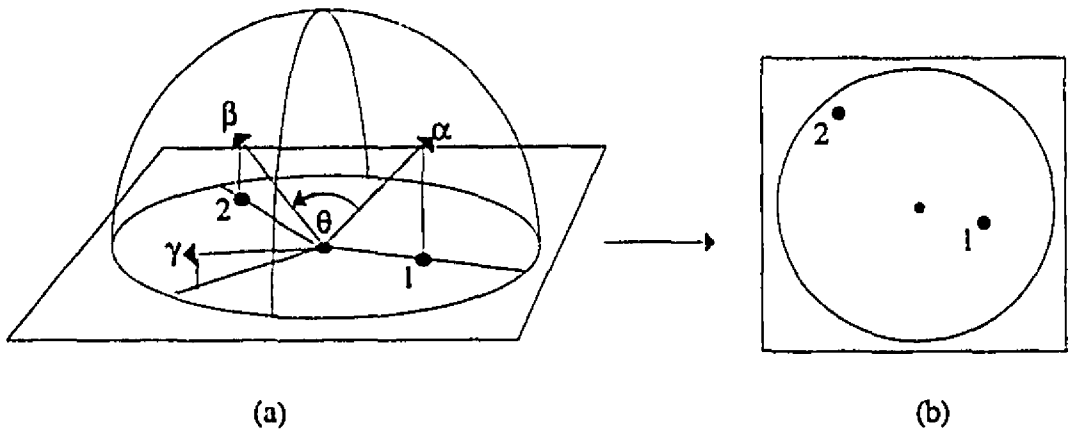

Figure 3.19. The concept of the virtual sphere view in 3-D (a) or in the drawn projection plane (b) .

Basic rotation tools are required to implement this algorithm. 4×4 transformation matrices are required. The fourth dimension of the matrix is required to carry the normalization needed to perform perspective projection and make objects appear bigger when they are closer.

An arbitrary point **p** is expressed as a row vector (p_x, p_y, p_z, 1). A translation matrix T is first needed to translate the point by an amount :$[t_x, t_y, t_z]$.

$$T = \begin{bmatrix} 1 & 0 & 0 & 0 \\ 0 & 1 & 0 & 0 \\ 0 & 0 & 1 & 0 \\ t_x & t_y & t_z & 1 \end{bmatrix} \tag{3.2}$$

The second step is to rotate the point. A matrix R that defines a rotation around a given axis (γ) by an angle θ is expressed as in [GLA0] by:

$$R = \begin{bmatrix} tx^2 + c & txy - sz & txz + sy & 0 \\ txy + sz & ty^2 + c & tyz - sx & 0 \\ txz - sy & tyz + sx & tz^2 + c & 0 \\ 0 & 0 & 0 & 1 \end{bmatrix} \tag{3.3}$$

where (x, y, z) is a unit vector along the direction of the rotation axis γ, with the parameters s, c and t defined as :

$$\begin{aligned} s &= \sin(\theta) \\ c &= \cos(\theta) \\ t &= 1 - \cos(\theta) \end{aligned} \tag{3.4}$$

Finally, the perspective projection matrix onto the x-y plane is defined as:

$$P = \begin{bmatrix} 1 & 0 & 0 & 0 \\ 0 & 1 & 0 & 0 \\ 0 & 0 & 0 & 1/Z_c \\ 0 & 0 & 0 & 1 \end{bmatrix} \tag{3.5}$$

Z_c is the Z distance between the center of projection and the observer's eye. Therefore the smaller Z_c is, the greater is the perspective effect.

The total transformation that incorporates a translation (T), a rotation (R) and a perspective (P) of one vertex $[v_x, v_y, v_z]$ of the object is given by:

$$[v_x', v_y', v_z', N] = [v_x, v_y, v_z, 1] \cdot T \cdot R \cdot P \tag{3.6}$$

Then, the point has to be normalized so that its fourth component is one, i.e.,

$$[V_x, V_y, V_z, 1] = \left[\frac{v_x'}{N}, \frac{v_y'}{N}, \frac{v_z'}{N}, \frac{N}{N}\right] \tag{3.7}$$

3.9.1 Real time rendering of the patient volume (Beam Eye's View)

Defining the patient's surface with triangular patches as described above makes possible the implementation of rendering when displaying the transformed (translated, rotated, and perspective projected) triangles. First, the triangles have to be translated so that the centre of rotation is the approximate centre of the patient's volume, although the center of rotation could be any point.

The simplest rendering technique, facet shading, was chosen. Facet shading means that every surface of an object has a uniform color which is proportional to the angle between the observer vector and the unit normal vector of that given surface. This information is readily available and the rendered color is rapidly computed. Each transformed triangle defines a polygon structure that can be framed or painted (direct Macintosh Toolbox Quickdraw drawing routines). The framing function allows wire frame display whereas painting with some appropriate color indexation allows rendering. Although there exist more realistic looking techniques for shading, like volume rendering, Gouraud shading [GOUR], Phong shading [PHON] and Interphong shading [ARVO], facet shading was chosen for its speed and simplicity. The more sophisticated techniques, though more realistic looking, require too much extra manipulation of the 3-D data, making the overall rendering process too slow for a real-time response on the current Macintosh computers .

The color indexation for the facet rendering is simply obtained through the dot product of the observer vector which corresponds to the normalization of (TçPçR[0][3]*Zc, TçPçR[1][3]*Zc, TçPçR[2][3]*Zc) vector with the unit normal of the particular surface which is stored in each triangular element. A color width and level for the display can be selected by normalizing the result of the dot product with a range of available color numbers in the color table; usually, the greater the dot product is, the lighter is the color, as if a light source came from the observer's position. The axis of the coordinate system reference frame can also be displayed so as to keep track of the position where the observer is looking from. Visualization of the beams (or boundaries of the beams) can also be shown. Many possibilities for the rendering are possible: the patient's skin could be wire-frame, facet rendered, or invisible. If the dot-product of a particular triangle with the observer's vector is positive, the skin is facing the observer, if negative, it faces the other side. The 3-D contours of the internal structures of interest can be drawn after drawing the background skin and before drawing a wire-framed surface giving the impression of a transparent skin (cf. Fig. 3.18 and 4.6).

3.9.2 Rotation of couch gantry set up (virtual treatment room)

Visualization of the 3-D position of the patient with respect to the treatment machine is easily achieved with the virtual sphere algorithm. However, more flexibility is required, since not only the capability of rotating the whole set-up is required but also the ability to rotate the couch and the gantry separately around their respective rotation axes. The couch and the gantry are both defined with three specific arrays. The first one contains a list of all the vertices of the object, the second contains the normal vector of all the surfaces, and the third contains the surface definition, i.e. a list of vertex numbers that forms each surface (four vertices per surface). Each object can now be rotated around its individual rotation axis or around an arbitrary axis defined through the virtual sphere algorithm with the isocentre position as centre of rotation. The visual output is shown in Fig. 3.20.

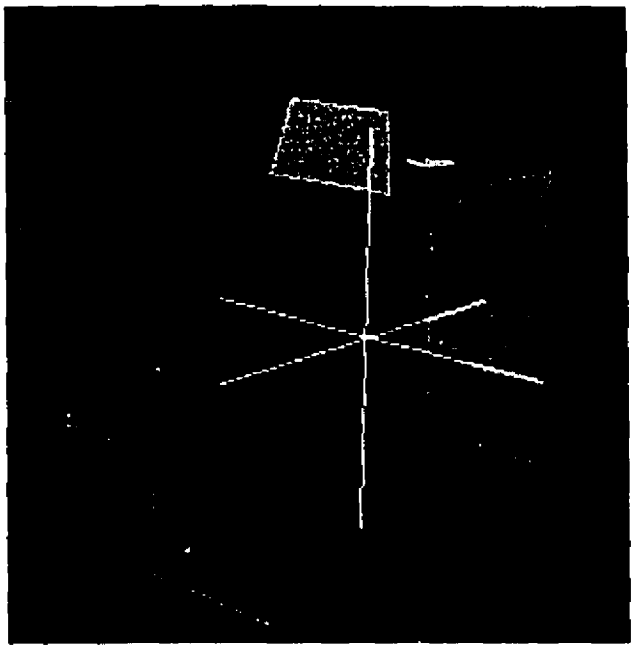

Figure 3.20. The couch and gantry visualization.

The dot-product of the observer normal and the normal of each surface (stored in the surface normal list) can also be used for real-time facet rendering as it was used for the patient surface. Wire frame display can also be selected.

Since the surfaces that constitute the couch and the gantry are larger than the patient's surfaces (small triangles) an additional operation is required before drawing the surfaces on the screen. A Z-sorting of the positioning of the surface themselves should be performed to avoid improper spatial superposition of couch and gantry parts. For simplicity, the painter algorithm was used. The surfaces are sorted by the sum of the z values of their vertices after transformation (proportional to the average z coordinate of the vertices of each surface). As long as the surfaces are small enough there is no problem in using this method. This explains why the top surface of the couch was actually split in 3 different parts. Other possibilities would have been to use Z-buffer based techniques [KIRK] that are memory consuming and in general slower since they involve rasterization of the surfaces. However a rasterization of the surfaces makes possible the use of the more realistic rendering techniques mentioned above.

Chapter 4

Results and Discussion

4.1 Introduction

The results of the implementation of the external photon beam treatment planning in the McGill Treatment Planning System will be presented here. The different windows pertaining to the different steps of a typical planning session will be discussed. Not every single window of the interface will be shown, the emphasis being on the newly implemented features. To ensure that the treatment planning program yields accurate calculation of the dose, measurements of the dose are presented and compared to the dose calculated by the computer. Finally, some limitations of the program are discussed to guide future work.

4.2 The planning interface

After the patient images are transferred through the computer network from the CT to a Macintosh computer they are loaded and converted to a 8-bit format by choosing a proper window width and level. The spatial location of each image plane is then entered along with the patient contour of each slice and the images are saved in a special compressed format, called "packed", that can be imported directly into the MPS program. Once the images are available in a usable format, they are loaded and placed in the image index window with the transverse image window showing the current active image The user can now use the contouring tools to draw the contours of the tumor and other structures of interest (cf. Fig. 4.1), always in the current image.

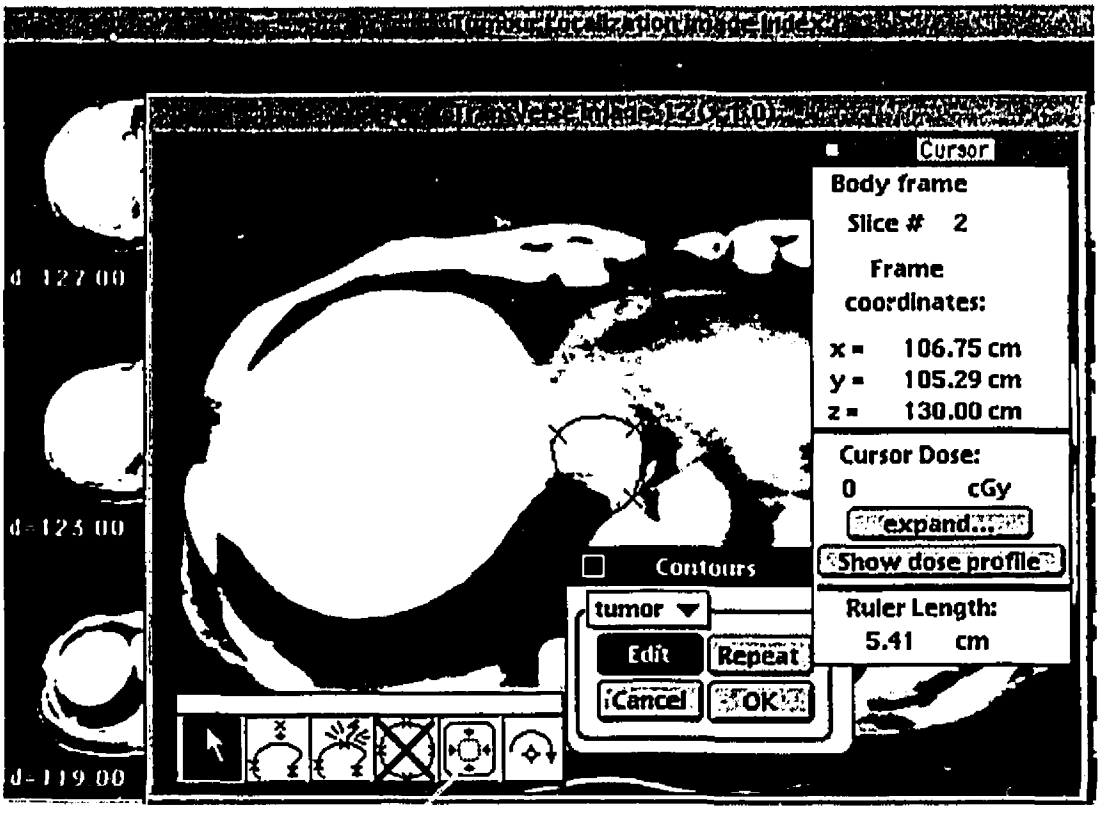

Figure 4.1. The planning interface just after loading the images and contouring the structures.

4.2.1. Treatment Parameters

Once all the contours have been drawn, the user defines the treatment parameters. First, the user has to decide where to place the isocentre, (for an SAD setup), or a point in the central axis of the beam for SSD setup. The image closest to that point is selected as the current image and the user clicks on the image at the isocenter position (while pressing a certain combination of keys). This operation opens a user dialog where the user sets the treatment parameters, (cf. Fig. 4.2).

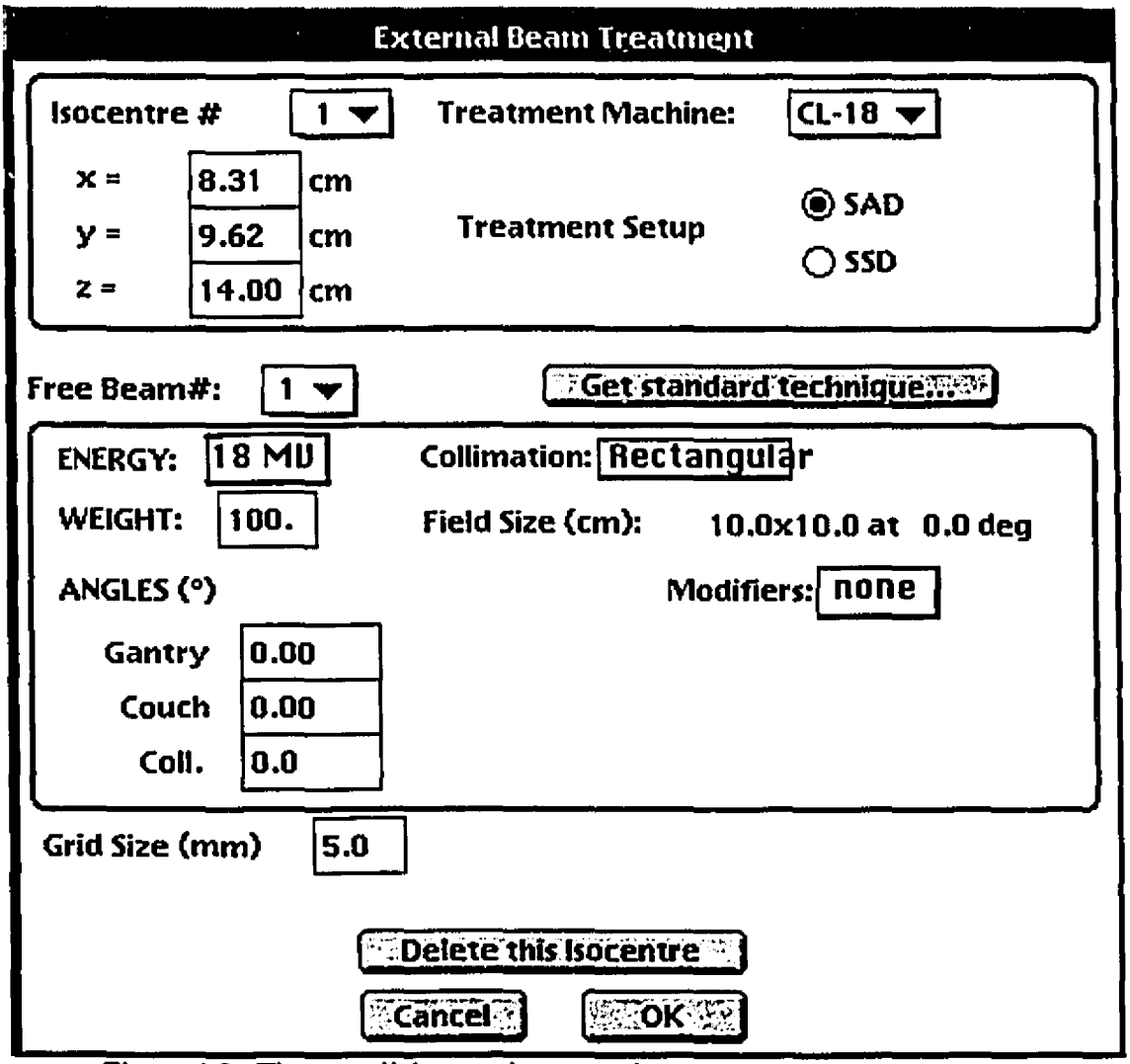

Figure 4.2. The user dialog used to enter the treatment parameters.

First the treatment set-up, (SSD or SAD) is chosen by clicking on the appropriate button in the dialog box. The choice of setup will change the normalization point for the dose calculation: the dose distribution is normalized to 100% at the isocentre point for an SAD set-up and at depth d_{max} along the central axis of the beam for the SSD setup. Then the treatment machine and type of radiation is selected through a pop-up that presents all the machine files that are present on disk. Certain machines, i.e., linear accelerators, may have more than one possible energy, and an additional pop-up menu in the dialog box allows the user to select among the different energies. The next step is to select the beam combinations and entry points for the particular treatment. Another pop-up menu lists all currently defined beams. Initially, no beams are defined. The user has to create new beams one by one or chose from previously defined general treatment techniques which may be composed of several predefined beams . When the beams are created one by one,

the user selects "new beam" from the pop-up menu and enters the various caracteristics for each newly created beam. Other functions are available to manipulate the beams; an already defined beam can be duplicated or removed from the beam list. The general techniques define a set of beams that compose a specific treatment technique. The general techniques that are available are: parallel-opposed beams, three beams at 120 , box technique (four beams at 90), and finally a dual field, i.e. open beam combined with wedged field, which is often used to obtain non-standard wedge angles. Modification of a beam requires that it is selected in the pop-up menu. All of its caracteristics can be changed, such as the collimator and gantry angles, the couch position and angle, the wedge angle (for wedged beam), the energy of the beam, and the type of collimation. So far the collimation types are rectangular and circular. There is an irregular field option planned for a future version of the program. For rectangular fields, the user must enter the length and width of the beam. Each beam can be treated as a pseudo-arc if desired. In this case, the user must enter the arc angle and the calculation step, i.e. how many fixed beams will approximate the rotation. The precise coordinates of the isocentre position can also be entered directly in frame coordinates. The calculation size for the grid can be modified, 5 mm being the default. The user can always cancel the modifications made to the treatment setting by clicking the "cancel" button in the window. Once the treatment is defined, the user exits and closes this window by clicking the "OK" button and all defined beams are then created. A cross-hair is now drawn on the transverse image window at the position of the isocentre. The dose at each point can be seen in the coordinate window by clicking at the requested point in the transverse image window. Before the isodose lines can be drawn , the dose at each grid point has to be calculated which is acomplished by selecting "dose calculation" in current slice from the pop-up menu. The progress of the calculation is shown with a progress bar dialog. Figure 4.3 shows the result of the calculation for a 4 beams box technique. This type of treatment takes less than 30 seconds per plane (image slice) to calculate, typically 5 to 10 seconds per beam. If the dose is also calculated in all image planes (all calculation grids), the isodose lines can be visualized as well in the coronal and sagital planes, as shown in Fig. 4.4.

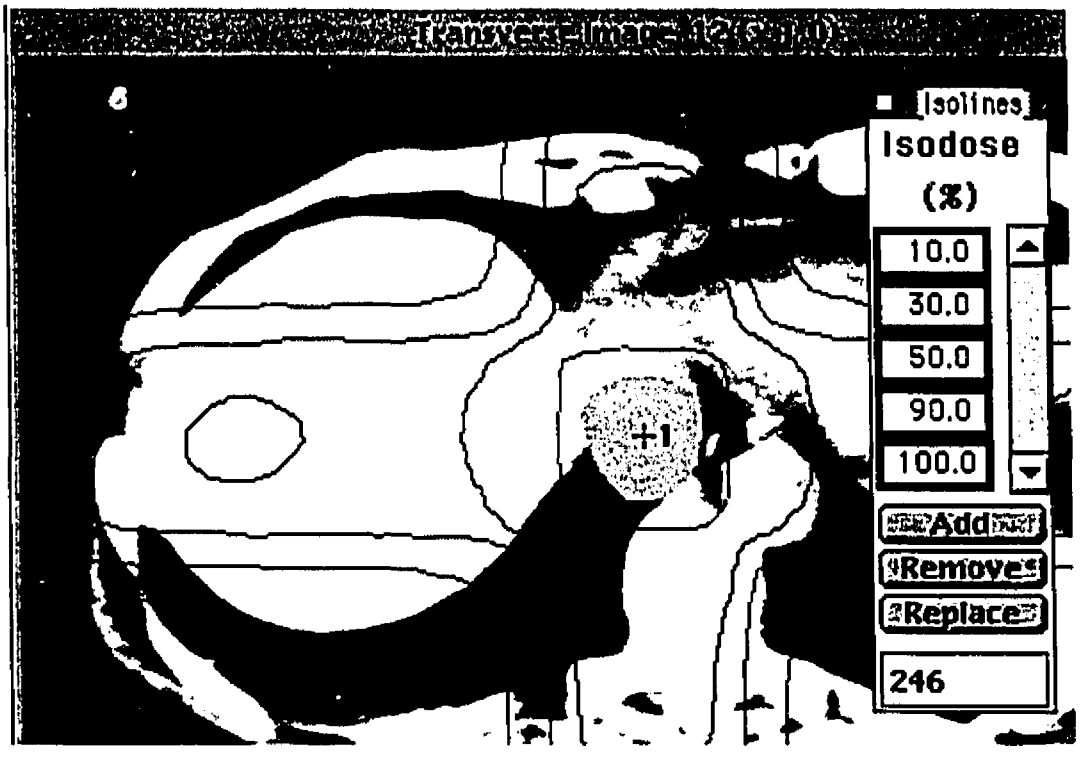

Figure 4.3. Dose calculation results, isodose lines in one image plane.

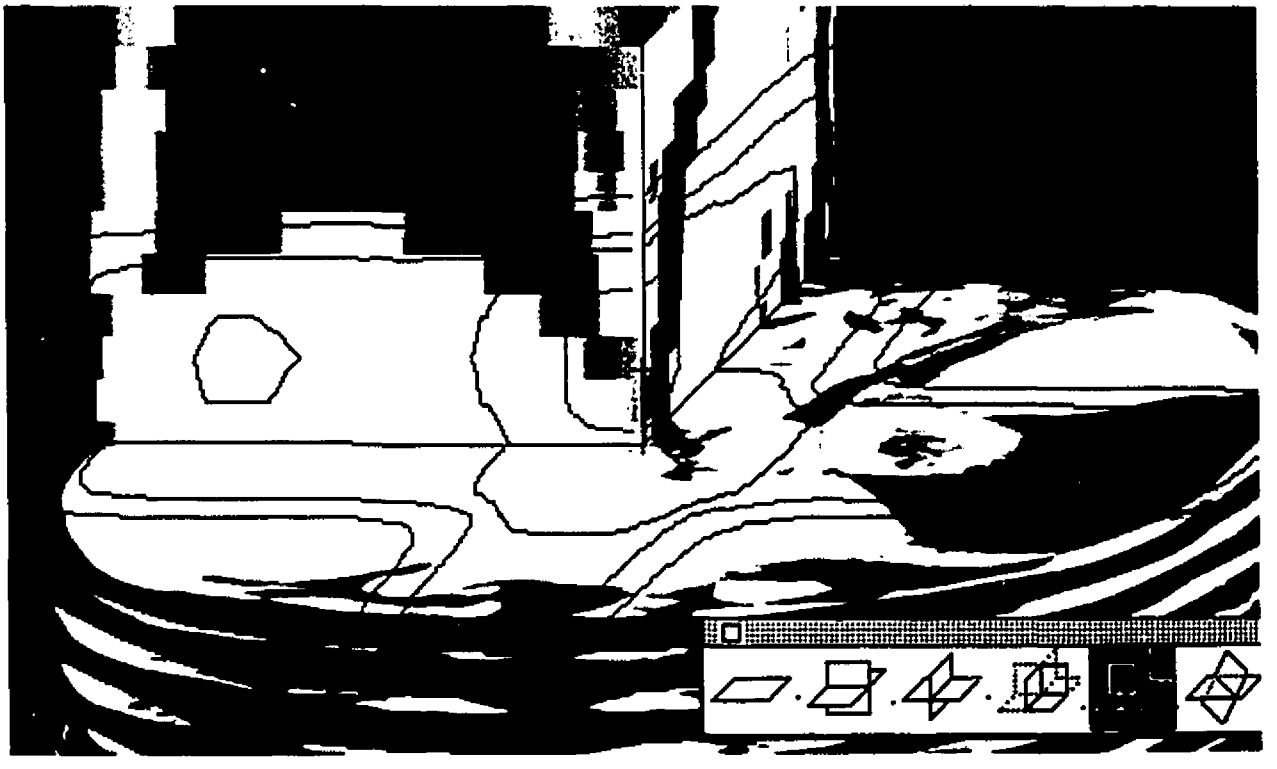

Figure 4.4. Reconstruction corner in the stack view window.

All tools that are available for stereotactic treatment planning are also available for external beam planning (dose volume histogram, beam eye's view, etc.). They are not shown here because they are not newly-created features.

However, as explained in Chapter 3, in order to extend the 3-D visualisation tools, an observer eye's view (OEV) was implemented. An example of the OEV display is shown in Fig. 4.6. The available display options are shown in Fig. 4.5. The user can set the surface that faces him or faces away in three modes: hidden, wireframe rendered or facet rendered. The user can also zoom in (or out) of the display. Options are left for future extensions such as viewing the intersection of the beam with the volume and displaying the structures of interest. It may also be possible in the future to show 3-D isodose surfaces when Macintosh computers will have greater calculation power or accelerated 3-D display cards. With the options implemented now, the display is normally fast enough for real time manipulation, i.e. the rotated object follows the mouse mouvement. However on old Macintosh computer models the response can be too slow; the user may then use a fast contour display to fix the viewing angle before doing the rendering.

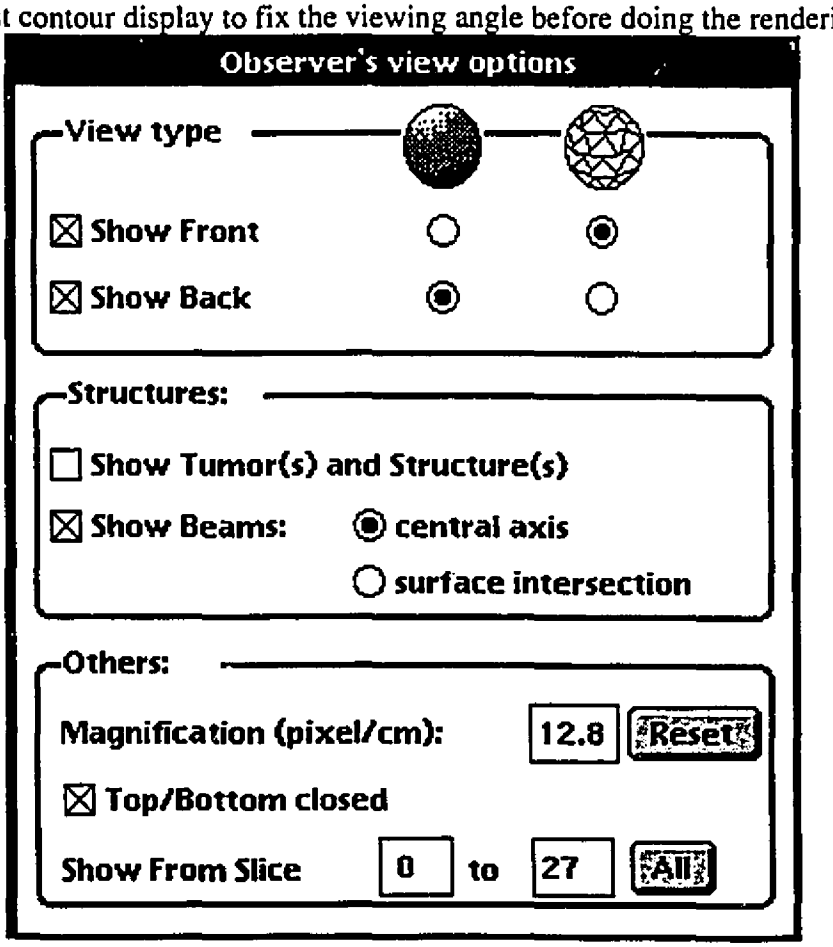

Figure 4.5. Dialog of options for the OEV display.

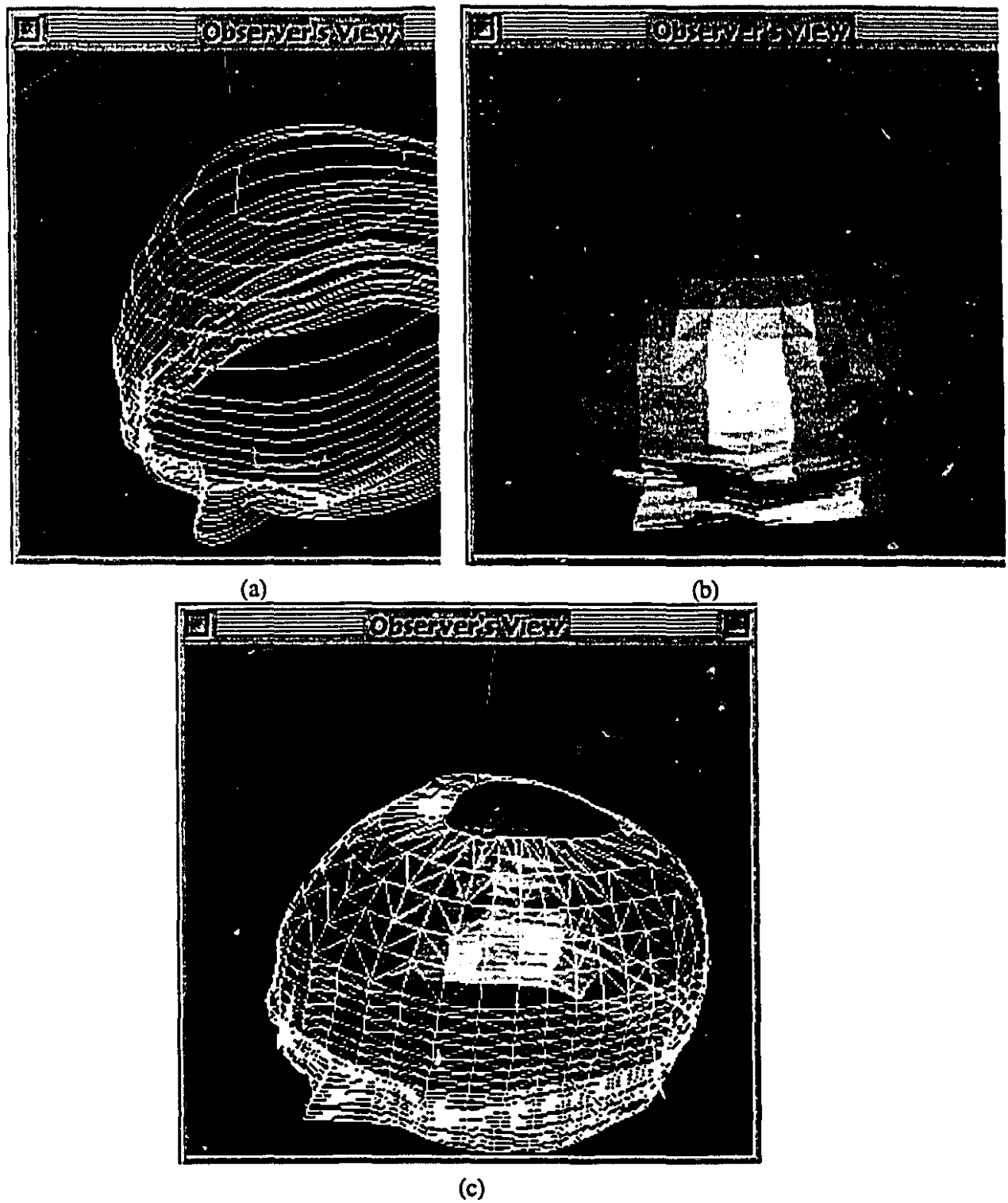

Figure 4.6. OEV display for a head images data set: (a) display of the contours for fast manipulation, (b) the facet rendered surface, (c) wire-frame surface and rendered background.

As the description of the user interface suggests, it is relatively easy to get a good idea of the dose distribution in 3-D and to interact with the program to evaluate the relative merit of different treatment plans.

4.3 Verifications of Results

A simple procedure for the verification of the calculation methods was followed. First, the measurements were performed in a homogeneous water phantom with the help of a radiation field analyser (RFA), (Therados RFA-7, Uppsala, Sweden). This device can be used as a three dimensional isodose plotter or as a two dimensional radiographic film densitometer. It is composed of a water-filled acrylic tank with dimensions of $63 \times 60 \times 61$ cm^3 and a set of p-type semiconductor detectors (Scanditronix, GR-p EC silicon photon field detector) and RK ionization chamber. One of the detectors can be positioned by remote-control anywhere within a $50 \times 50 \times 50$ cm^3 volume while the other is used as a stationary reference detector. The relative signal strength, which is proportional to the dose, is recorded by the computer control unit (80186, 16 bit processor), and saved on disk as a text file.

The measurements of PDD values along the central axis of the beam and the measurement of the dose profiles along the central plane of the beam at various depths (cf. Fig. 4.7) were obtained with the RFA. All measurements were taken for the energy that was verified (18 MV). The relative dose measurements are normalized to 100% at depth d_{max} (3 cm).

For verification of oblique incidence correction, some beam profiles were imaged on film (Kodak X-Omat V) with 30 cGy given at d_{max} to ensure that the optical density of the film varies linearly with the dose (Fig. 4.8). The films were placed in between polystryrene sheets (3.24×10^{23} electrons/gram, 1.03 g/cm^3) which are assumed to be water equivalent material (3.34×10^{23} electrons/gram, 1.00 g/cm^3). The films were digitized with a CCD camera to 8-bits images. A calibration curve for dose versus pixel density was then obtained with a reference film of a 10×10 cm^2 beam at normal incidence (cf. Fig. 4.9) comparing PDD measurements values with pixel values along the central axis on the image. The calibration curve was aproximated by a third degree polynomial fit and it was used to convert pixel value to dose. Image manipulations were

performed with NHI-Image software package for Macintosh [NIHI]. The program allows distance calibration (pixel/cm) and color calibration (pixel color to dose calibration from the fit) to be applied to an image. Therefore dose profiles along any line of the calibrated images are readily available.

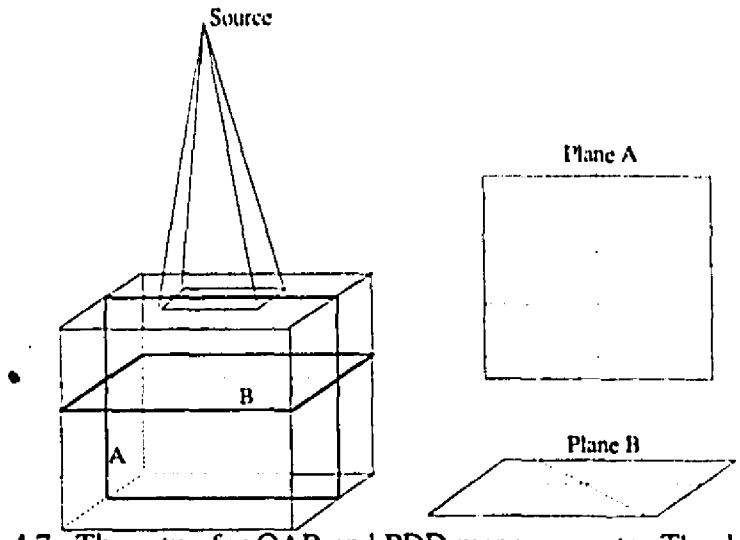

Figure 4.7. The setup for OAR and PDD measurements. The dashed lines in the measurement planes represent the lines along which measurements were taken.

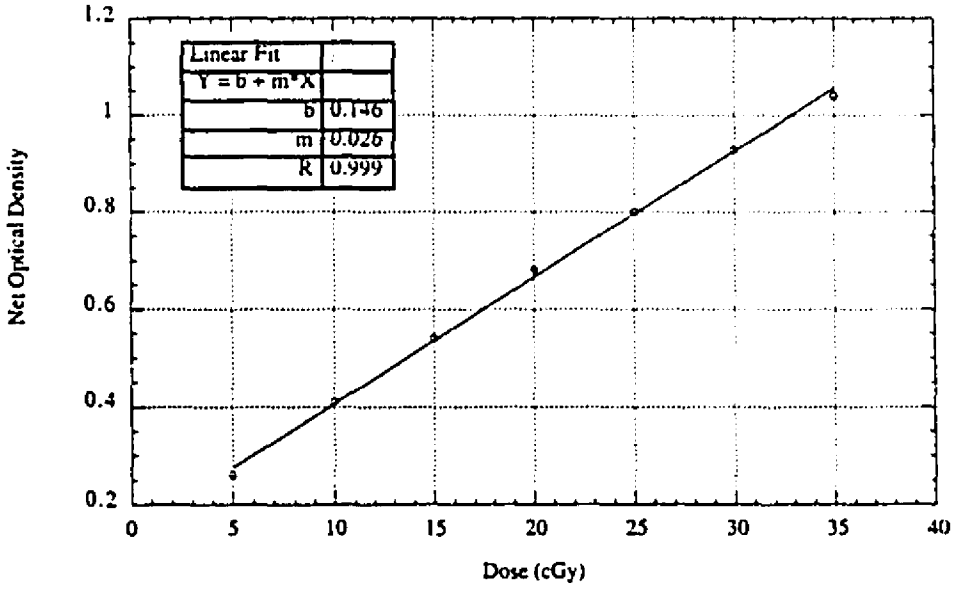

Figure 4.8. Optical density read on a Kodak X- Omat V film versus given dose in the linear region (5 to 35 cGy) for 18 MV photon radiation.

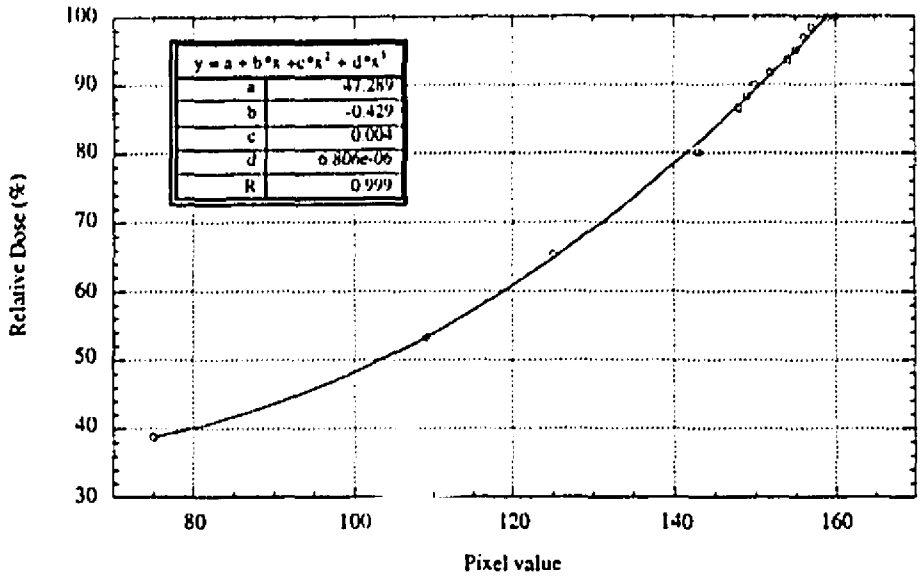

Figure 4.9. Polynomial fit for conversion of pixel value to relative dose for Kodak X-Omat V film scanned with a CCD camera (18 MV photon radiation).

4.3.1 Verification with RFA measurements

1- Normal incidence at SSD distance of measured data

The percentage depth dose and off-axis ratio used as input data were verified to be consistant with the calculated value. Since the input data is manipulated for efficient storage and converted to TMR values (the dose calculation procedure uses TMR values), the first step in verifying the calculation is to compare calculation of dose (Eq. 2.34) for a setup that is exactly the same as the input data, i.e. SSD = 100 cm normal incidence on a cubic phantom for 18 MV photon radiation. The PDD curve and the off-axis ratio at four of the measured depths, 3 cm, 11 cm 19 cm and 27 cm, were verified for a 10×10 cm^2 field, The difference between the measured and the calculated dose values is less than one percent as shown in Figures 4.10. and 4.11

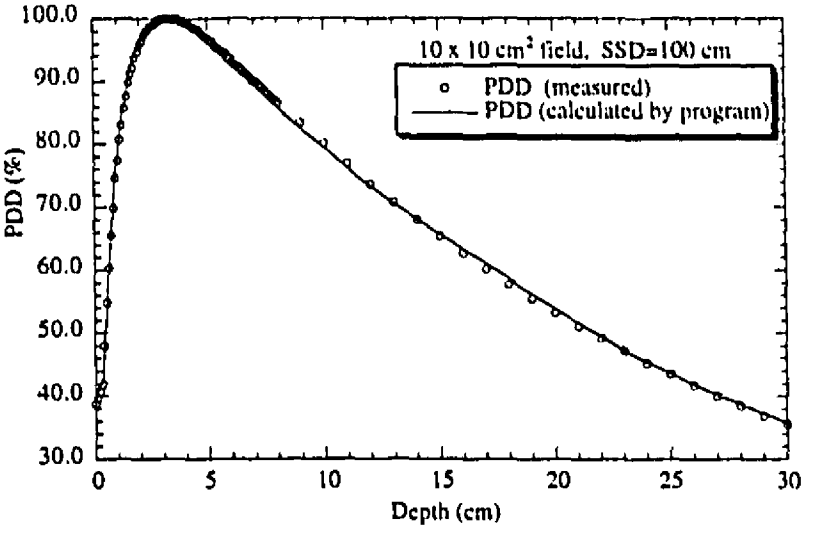

Figure 4.10. Percent depth dose verification for a 10 × 10 cm^2 field SSD = 100 cm, 18 MV photon radiation.

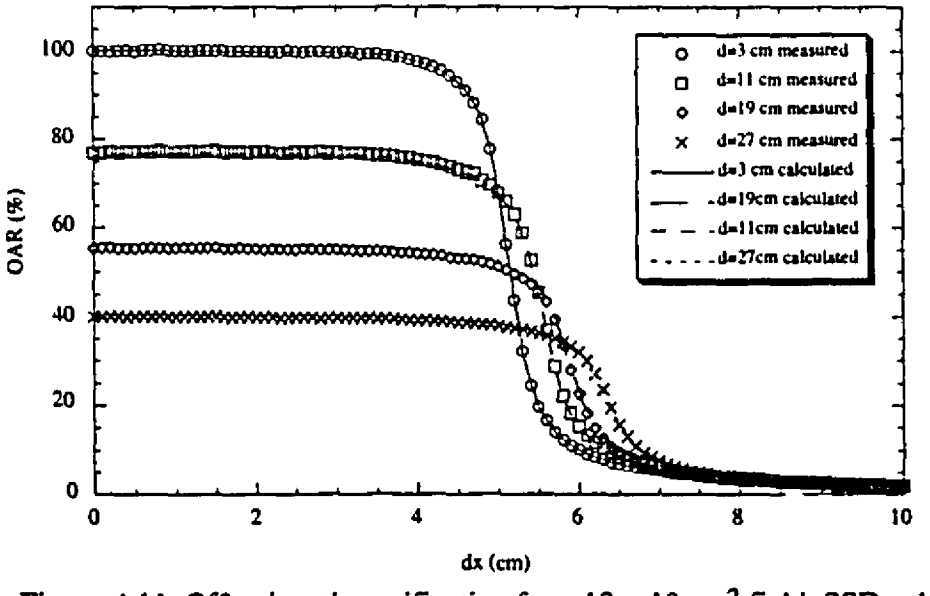

Figure 4.11. Off-axis ratio verification for a 10 × 10 cm^2 field, SSD = 100 cm, 18 MV photon radiation.

2- Correction for beam divergence for different SSD

Next, the correction for the beam divergence was verified (cf. Eq. 2.35) when the setup is not at the SSD of the measured data. Figures 4.12. and 4.13 show the beam profiles for two different SSD, 90 and 80 cm again for a 10×10 cm^2 beam at 4 different depths (3, 11, 19 and 27 cm). The difference between the measured and calculated dose values is less than the acceptable 2% in clinically significant regions [ICR4].

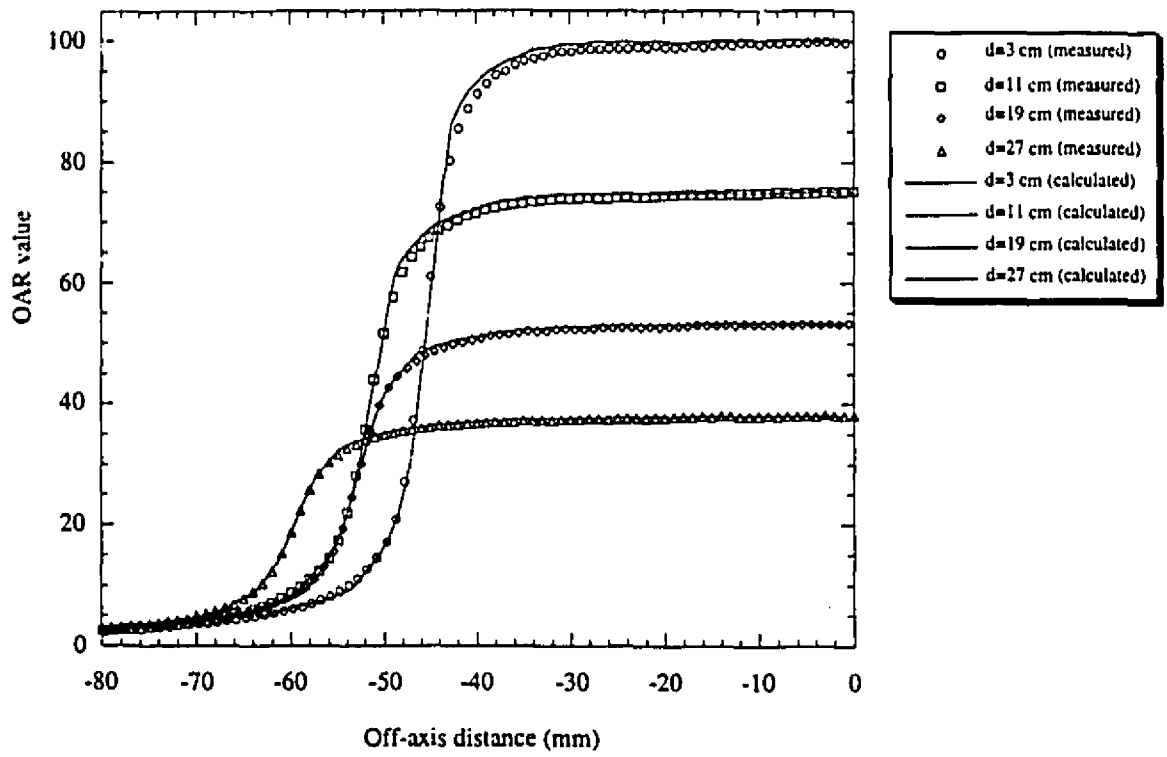

Figure 4.12. Comparaison of calculated and measured profile at SSD = 90 cm for a 10×10 cm^2 beam.

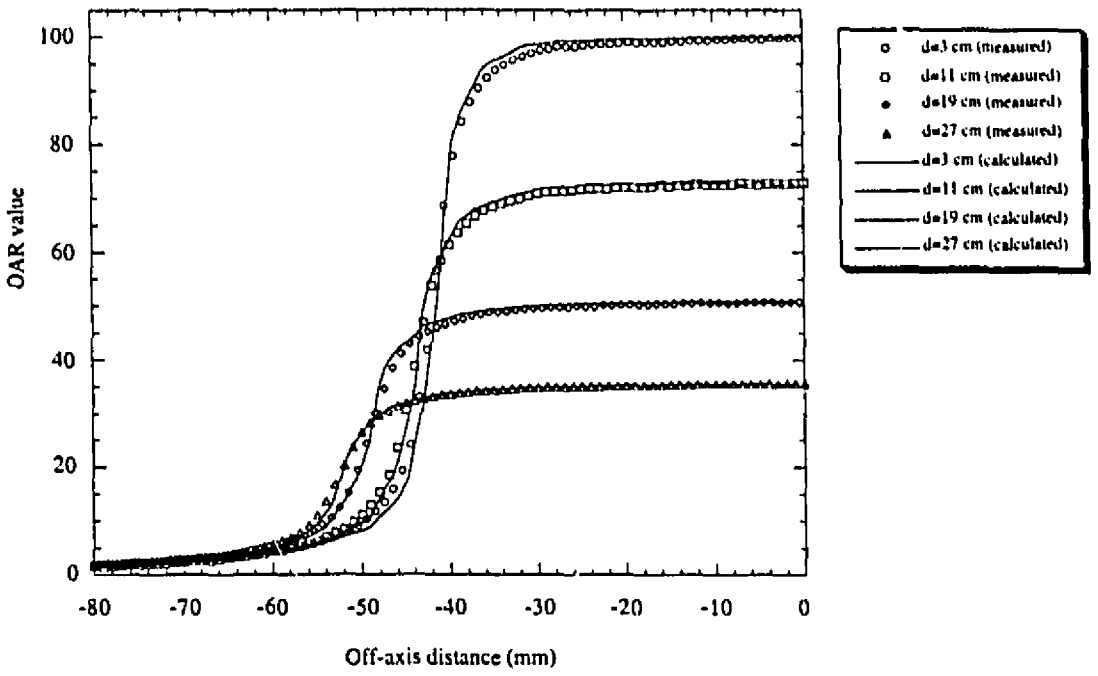

Figure 4.13. Comparaison of calculated and measured dose profiles at SSD = 80 cm for a 10 × 10 cm^2 beam, 18 MV photon radiation.

3- Verification of off-axis correction method

The validity of the off-axis value calculation given by Eq. 2.15 was verified by comparing calculated and measured normalized dose values along the diagonal (diagonal line of plane B of Fig. 4.7) of both a 10 × 10 cm^2 and a 30 × 30 cm^2 beam at four different depths (3, 11, 19 and 27 cm). The difference between the measured and calculated values is less than 2 % everywhere except for some points in the penumbra region (cf. Fig. 4.14 and 4.15). In general, the calculated dose is underestimated in the penumbra region and overestimated in the "horns" regions. This is a direct result of the multiplicative rule of Eq. 2.15. In general, non flat beam dose profiles will be reproduced adequately in the central planes because the profile values are normalized to 1 on these planes at the central axis, but in other planes (diagonal planes) it will exaggerate the non-flatness of the beam. For wedged beam, the multiplicative rule will use the open beam for the dose profile on the length direction of the wedge and the wedged beam profile in the lateral direction; this method will yield larger errors since it does not take into account the effect of beam hardening and scattering by the wedge.

Therefore the current method for off-axis correction should not be used directly with wedged fields. More verifications should be performed and an alternate method for that type of correction should be used, such as the one discussed in Chapter 2.

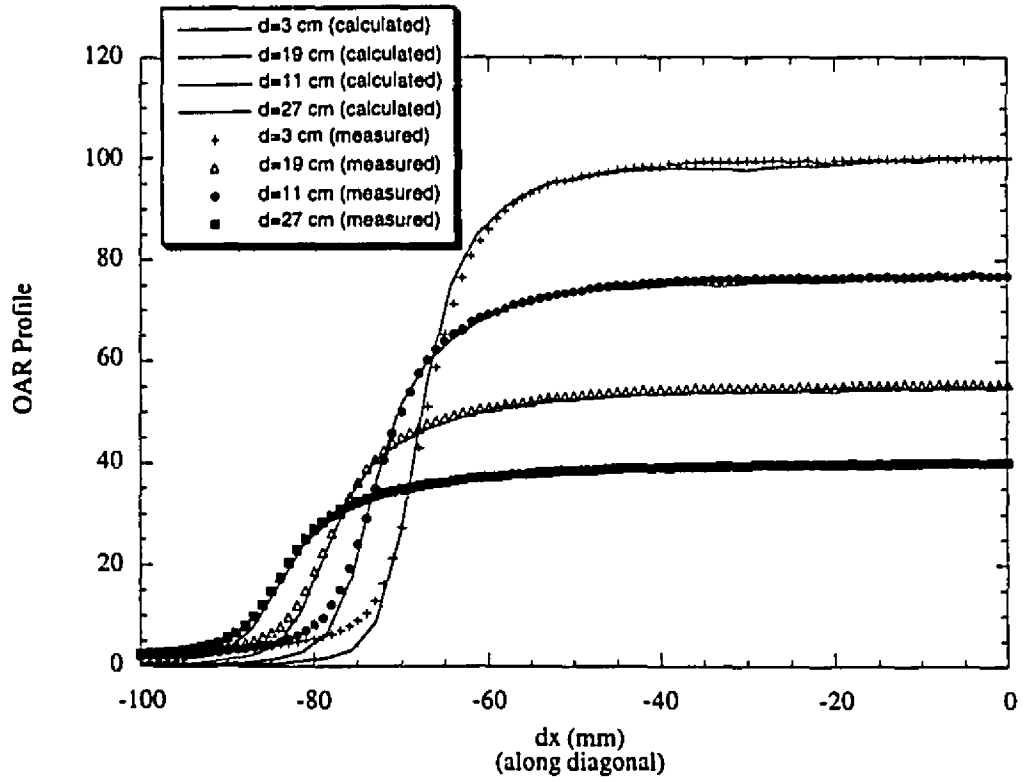

Figure 4.14. Profiles along the diagonal axis of a 10 × 10 cm^2 field at various depths for 18 MV photon radiation.

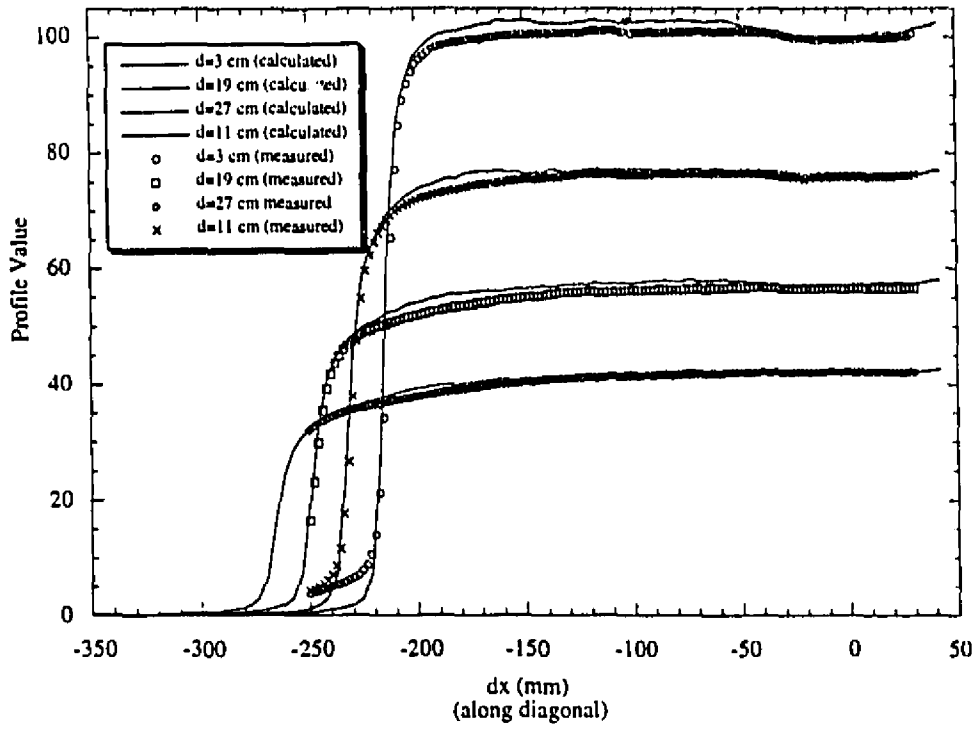

Figure 4.15. Profiles along the diagonal axis of a 30 × 30 cm^2 field at various depths for 18 MV photon radiation.

4.3.2 Verification of oblique incidence correction with film Dosimetry

For testing the validity of using the slant depth as the depth d in Eq. 2.33 to correct for surface curvature, film was used to measured beam profiles along the central axis of the beam at various depths for two beam angles incidence (10 and 20) following the above procedure. These measurements were compared to values calculated with the program (cf Fig. 4.16 and 4.17). Despite the relatively noisy measured profiles their agreement with the calculation is quite good since they differ by less than the acceptable 2%. The large difference in the penumbra region is explained by the pixel value to relative dose conversion from the fit of Fig. 4.9 which is not valid in regions with relative dose less than 10%. Measurement of dose with film in regions receiving very low dose (less than 5 cGy) are difficult because the optical density produced by low dose is comparable to the background optical density of the film. Also in these regions the energy response of the film is not linear.

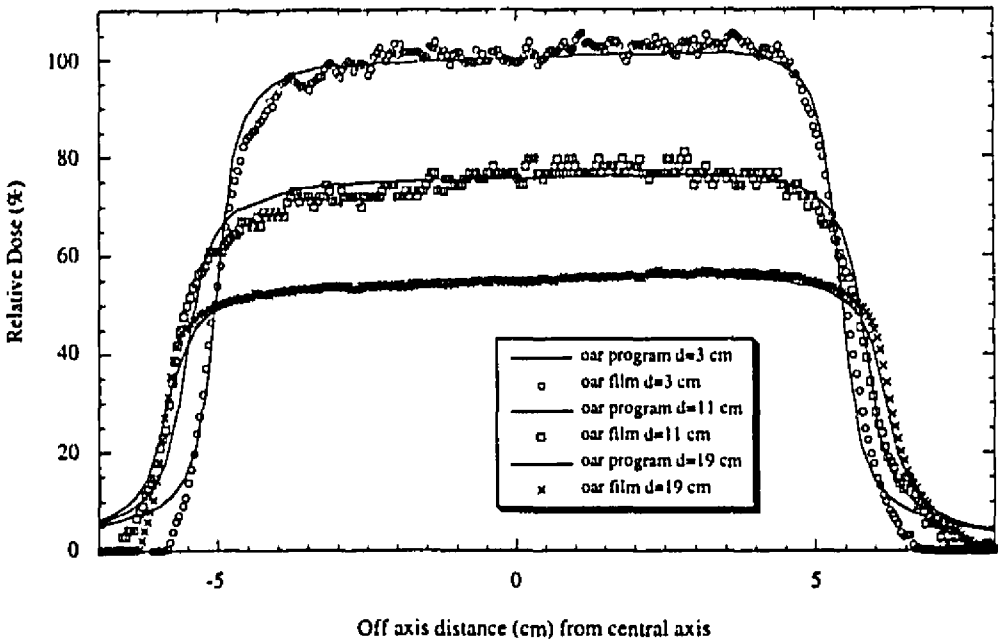

Figure 4.16. Relative dose profiles measured with film and calculated with the program for oblique 10 incidence, 10 × 10 cm^2 field at three different depths.

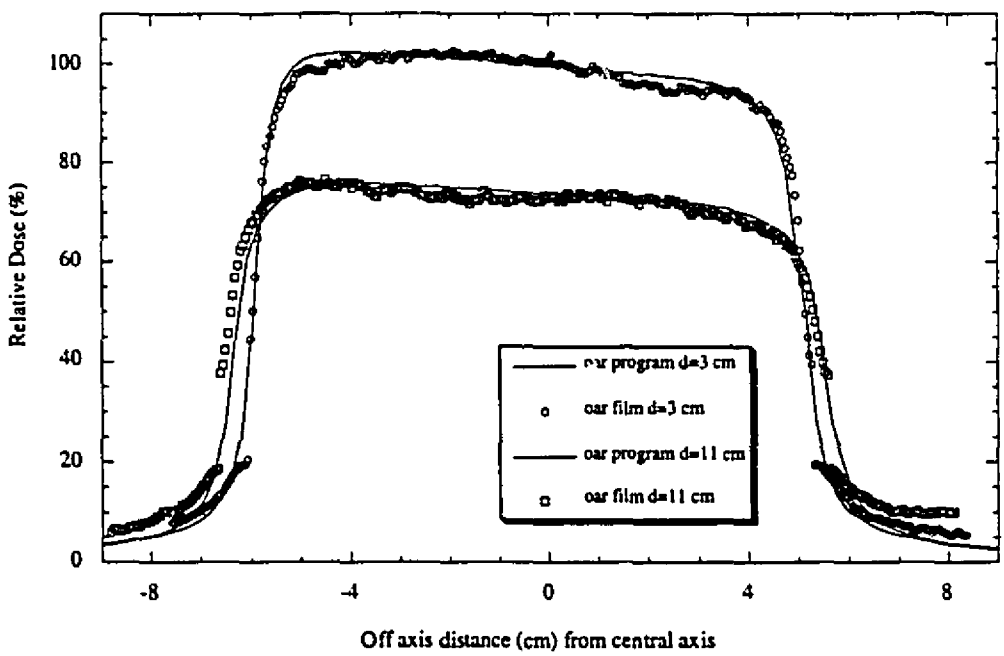

Figure 4.17. Relative dose profiles measured with film and calculated with the program for oblique 20 incidence, 10 × 10 cm^2 field at two different depths.

4.4 Discussion and future work

The dose calculation algorithm that was implemented yields accurate calculations in homogeneous water-equivalent material for typical clinical beam setups. The methods to correct for oblique incidence of the beam and for beam divergence were shown to be adequate. The correction of the off-axis ratio values was also shown to be acceptable for non wedged beams. Even if the measured and calculated relative dose differ by a few percent in the penumbra region for some of our results (in particular with films measurements), this is not to be consider as a problem: in external beam treatment planning the treatments are usualy composed of several beams and the contribution to the total dose from the penumbra region of each beam is less than one percent of given dose to the isocentre. The differences measured with the ionization chamber measurents are within 5 %, and with the films measurements the difference is not applicable since in these regions the energy response of the film is not linear.

The interface of the program is relatively straight-forward, giving the user the possibility to interact with the program easily and rapidly through all steps of a planning session, from importing images and defining contours to the visualization of the dose and creation of the treatment plan.

The program is a good starting point that has all the basic tools for external beam treatment planning. However there are some limitations to the current work. Future implementation could improve the performance and the quality of the planning. First of all, the planning interface could be improved by using a graphical palette tool with which the user could easily select tools to create and directly manipulate graphically the various treatment beams instead of using the user dialog of Fig. 4.2. The visualisation of the dose should also be available in any arbitrary reconstructed image plane: the viewing is now limited to transverse, coronal and sagittal planes. A graphical interface for entering new beam data would be very useful and save time compared to the current method of creating a properly formatted text file. The observer eye's view could be completed to view tumor and other internal structures along with the intersections of the beams on the treated volume surface. This interface could also be used to select and manipulate directly the beams in three dimensional space.

Before using the program to do external beam treatment planning in a clinic, the dose calculation should be extended to handle irregular fields and heterogeneity corrections.

These corrections should be verified by comparing actual measurements with the calculations. Systematic verification of all input data should be performed to avoid entry errors. The off-axis correction procedure should be verified with wedged fields to confirm whether the multiplicative rule of Eq. 2.15 is applicable or should be replaced by the method discussed in Chapter 2.

As the computation power of personal computer is constantly increasing, the implementation of more sophisticated algorithms would certainly be a solution to consider within a few years. However in the mean time, the current implementation of 3D external photon beam treatment planning for the McGill Treatment Planning System is very appropriate, despite the discussed limitations, and completes the planning capabilities of the system.

Chapter 5

Conclusions

5.1 Summary

An user interface and the required algorithms to perform 3D external photon beam treatment planning have been implemented in the McGill Treatment Planning System program. Treatment planning theory and the problem of calculating the dose in a treated volume was discussed. Continuous improvements in computer technology have had an enormous influence in the quality of the treatment planning procedure by fixing the standards. The development of user interfaces and computer graphics have simplified the manipulation of data and have opened new capabilities for visualizing treament plans and patient data images, or volumes, acquired from medical scanners. The consequence of computerized treatment planning is that not only the planning task has been greatly simplified, but also the accuracy of the dose calculation has been drastically improved. Another major consequence is that standard treatment planning programs can now be run on relatively inexpensive personal computers.

The work of this thesis consisted in implementing the basic algorithms to perform 3-D photon beam treatment planning with the existing McGill Treatment Planning System. This system runs on standard Macintosh personal computers (PowerPC or 68K models). The source code is in C programming language compiled with CodeWarrior C/C++ρ compiler from MetroWerks Inc. A dose calculation procedure that uses measured beam data as input parameters (percent depth dose curves and off-axis ratio) was implemented. Corrections for beam divergence and oblique incidence were shown to be adequate to calculate the dose for typical clinical beams, with a difference less than 2% between the measured and calculated points in clinically important regions. Work has also been done to create an observer eye's view display and a 3-D model of the treatment room set-up. This display offers a configurable easy to use interface for visualizing the 3-D patient data set in space in conjunction with the treatment set-up.

However, before this external photon beam treatment planning program can be used in the clinic, verification with wedged field beams should be performed. Moreover, a calculation procedure should be implemented to calculate the dose from irregular fields and the possibility to use a correction method to account for heterogeneity structures should also be offered.

BIBLIOGRAPHY

[AAP1] AAPM Task Group 21, *A protocol for the determination of absorbed dose from high-energy photon and electron beams,* Med. Phys. **10**, 741 (1983)

[AAP2] AAPM Task Group 25, *Clinical electron beam dosimetry*, Med. Phys. **18**, 73-109 (1991)

[ANDR] Andreo, P., *Monte Carlo techniques in medical radiation physics*, Phys. Med. Biol. **36**, 861-819 (1991).

[ARVO] Arvo J., Graphics Gems II , Academic Press Limited, USA, (1991)

[ATTI] Attix F.H., Introduction to Radiological Physics and Radiation Dosimetry., John Wiley & Sons, Toronto, Ontario (1986)

[BEN0] Bentel, G., Radiation Therapy Planning. McGraw-Hill Inc., Health Profession division. (1992)

[BEN1] Bentley R.E., *Digital Computers in Radiation Treatment Planning*, Brit. J. of Radiol., **37**, 748-755 (1964)

[BEN2] Bentley, R.E., Milan J., *An interactive digital computer system for radiotherapy treatment planning*, Brit. J. of Radiol., **44**, 826-833.(1971)

[BRAM] Brahme, A., *Dosimetric requirements in radiation therapy*, Acta Radiol. Onctol. **23**, 379-391, (1984).

[CARO] Carol, Mark P., *Peacock™: a System for Planning and Rotational Delivery of Intensity-Modulated Fields*, Int. J. of Imaging System and Technology, **6**, 56-61 (1995)

[CHEN] Chen M., *A study in interactive 3-D Rotation Using 2-D Contol Devices*, Computer Graphics, **22**, 121-129 (1988)

[CHIN] Chin L.M., Siddon R.L., Svensson G.K., Rose C. : *Progress in 3-D treatment planning for photon beam therapy*, Int. J. Radiation Oncology Biol. Phys., **11**, 2011-2020 (1985)

[CHU1] Chui, C., Mohan, R., *Off-center ratios for three-dimensional dose calculations*, Med. Phys. **13**, 409 (1986)

[CLAR] Clarkson, J.R., *Note on depth doses in fields of irregular shape,* Brit. J. Radiol. **14** 265-268. (1941)

[CUN0] Cunningham, J.R., *Tissue Heterogeneity characterization and corrections,* (AAPM Monograph No 9), 292-309 (1983)

[CUN1] Cunningham, J.R., Battista, J.J., *Calculation of dose distributions for x ray therapy*, Physics in Canada, **51**, 190-195 (1995)

[DAYA1] Day, M.J., Aird, E.G.A., *The Equivalent-Field Method For Dose Determinations in Rectangular Fields* , Brit. J. Radiol., Supplement **17**, 105-114, (1983)

[EVAN] Evans R.D., The Atomic Nucleus, Frieger Publishing, (1955).

[GLA0] Glassner A.S., Graphics Gems Academic Press Limited, USA, (1990)

[GLA1] Glassner A.S., Graphics Gems IV , Academic Press Limited, USA, (1990)

[GOI1] Goitein M., Abrams M., *Multi-dimensional treatment planning I: Delineation of Anatomy* , Int. J. Radiation Oncology Biol. Phys. , **9**, 777-787 (1983)

[GOI2] Goitein M., Abrams M., Rowell D., Pollari H., and Wiles J., *Multi-dimensional treatment planning II: Beam's Eye-view, back projection and projection through CT sections*, Int. J. Radiation Oncology Biol. Phys. ,**9**, 789-797 (1983)

[GOI3] Goitein, M., *Limitations of the two dimensional treatment planning program*, Med. Phys., **9**, 580-586, (1982)

[GOI4] Goitein, M., *Applications of computed tomography in radiotherapy treatment planning*, Chapter 4 of Progress in Medical Radiation Physics Volume 1, Ed. C.G. Orton, Plenum Publishing Co. New York. (1982)

[GOUR] Gouraud H., *Continuous shading of curved surfaces*, IEEE Trans. Comp. **20**, 623-628. (1971)

[HOUN] Hounsfield, G.N., *Computerized transverse axial scanning (tomography)*, Brit. J. of Radiol., **46**, 1016 (1973)

[ICR1] ICRU, Clinical Dosimetry, Washington DC, International Commission on Radiation Units and Measurements, Report 10b, (1962).

[ICR2] ICRU, Determination of Absorbed Dose in a Patient Irradiated by Beams of X or Gamma Rays in Radiotherapy Procedures, Washington DC, International Commission on Radiation Units and Measurements, Report 24 (1976).

[ICR3] ICRU, Dose Specifications for Reporting External Beam Therapy, Washington DC, International Commission on Radiation Units and Measurements, Report 29, (1979).

[ICR4] ICRU, Use of Computers in External Beam Radiotherapy Procedures with High Energy Photons and Electrons, Washington DC, International Commission on Radiation Units and Measurements, Report 42 (1987).

[JOCU] Johns H.E., Cunningham J.R., Physics of Radiology ,4th edition. C.C. Thomas, Springfield, Illinois, U.S.A. (1983)

[KHAN] Khan, M.F., The Physics of Radiation Therapy, 2nd edition. Williams and Wilkins, Maryland, U.S.A. (1984)

[KIRK] Kirk D., Graphics Gems III , Academic Press Limited, USA, (1992)

[LAUR] Laurent J.P., Mehaute A., Schunaker L.L., Curves and Surfaces, Academic Press Inc. USA (1991)

[MACK] Mackie, T.R., Bielajew, A.F., Rodgers, D.W.O., Battista, J.J., *Generation of photon energy deposition kernels using the EGS4 Monte Carlo code*, Phys. Med. Biol. **33**, 1-20, (1988).

[MILA] Milan J, Bentley, R.E., *The Storage and manipulation of Radiation Dose Data in a Small Digital Computer*, Brit. J. of Radiol., **47**, 115-121.(1974)

[MOHA] Mohan R., Barest G., Brewster L.J., Chui C.S., Kutcher G.J., Laughlin J.S., and Fuks Z., *A comprehensive three dimensional radiation treatment planning system*, Int. J. Radiation Oncology Biol. Phys., **15**, 481-495. (1988)

[NIHI] NIH-Image 1.59 software, programmed by Rasband, W., National Institute of Health, U.S.A. (1995).

[PCW1] Photon Treatment Planning Collaborative Work group, *State of the Art of External Radiation Treatment Planning*, Int. J. Rad. Onc. Biol. Phys., **21**, 9-23. (1993)

[PCW2] Photon Treatment Planning Collaborative Work group, *Three Dimensional Dose Calculations For Radiation Treatment Plannning*, Int. J. Rad. Onc. Biol. Phys., **21**, 25-35. (1993)

[PCW3] Photon Treatment Planning Collaborative Work group, *Interinstitutional Experience in Verification of External Photon Dose Calculations*, Int. J. Rad. Onc. Biol. Phys., **21**, 37-58 (1993)

[PHON] Phong, B.T., *Illumination for computer generated images*, Ph.D. Dissertation, University of Utah. (1973)

[PLA1] Pla, C., *A Macintosh based treatment planning system for brachytherapy and stereotactic radiosurgery*, Proceeding of the XIthe International conference on the use of computers in radiation therapy, 138-139. (1994)

[ROD1] Rogers, D., *Fundamentals of high energy x-ray and electron dosim. protocols*, AAPM Monograph 19, (1991)

[ROGE] Rogers D. F., Adams J.A., Mathematical elements for computer graphics, 2nd edition, McGraw Hill, USA, (1990)

[SID1] Siddon R. L., *Calculation of the radiological depth*, Med. Phys. **12**, 84-87.(1985)

[SID2] Siddon R. L., *Fast Calculation of the exact radiological path for a three-dimensional CT array*, Med. Phys. **12** , 252-255.(1985)

[SID3] Siddon R.L., *Prism representation: a 3D ray -tracing algorithm for radiotherapy applications* , Phys. Med. Biol., **30** , 817-824.(1985)

[SONT] Sontag, M.R., Cunningham, J.R., *The equivalent tissue-air ratio method for making absorbed dose calculations in a heterogeneous medium*, Radiology, **129**, 787-794, (1978).

[STAR] Starkschall G., *Analytical evaluation of depths of dose calculation points for external beam radiation therapy treatment planning*, Med. Phys. , **12**, 477-479 (1985)

[STER] Sterling, T.D., Perry H., Katz L., *Automation of radiation treatment planning*, Br. J. Radiol. **37**, 544, (1964)

[TSIE] Tsien, K.C., *The application of automatic computing machines to radiation treatment planning*, Brit. J. of Radiol., **28**, 432-439 (1955)

[WON1] Wong, J.W., Henkelman, R.M., *A new approach to CT pixel based photon dose calculations in heterogeneous media*, Med. Phys. **10**, 199-208, (1983)